INFORMATION TO USERS

This dissertation was produced from a microfilm copy of the original document. While the most advanced technological means to photograph and reproduce this document have been used, the quality is heavily dependent upon the quality of the original submitted.

The following explanation of techniques is provided to help you understand markings or patterns which may appear on this reproduction.

1. The sign or "target" for pages apparently lacking from the document photographed is "Missing Page(s)". If it was possible to obtain the missing page(s) or section, they are spliced into the film along with adjacent pages. This may have necessitated cutting thru an image and duplicating adjacent pages to insure you complete continuity.

2. When an image on the film is obliterated with a large round black mark, it is an indication that the photographer suspected that the copy may have moved during exposure and thus cause a blurred image. You will find a good image of the page in the adjacent frame.

3. When a map, drawing or chart, etc., was part of the material being photographed the photographer followed a definite method in "sectioning" the material. It is customary to begin photoing at the upper left hand corner of a large sheet and to continue photoing from left to right in equal sections with a small overlap. If necessary, sectioning is continued again — beginning below the first row and continuing on until complete.

4. The majority of users indicate that the textual content is of greatest value, however, a somewhat higher quality reproduction could be made from "photographs" if essential to the understanding of the dissertation. Silver prints of "photographs" may be ordered at additional charge by writing the Order Department, giving the catalog number, title, author and specific pages you wish reproduced.

University Microfilms

300 North Zeeb Road
Ann Arbor, Michigan 48106

A Xerox Education Company

72-27,104

SHORT, David Winfield, 1945-
THE INFLUENCE OF SURFACE CHARGE AND SURFACE STRUCTURE ON THE SUBLIMATION OF IONIC CRYSTALS.

The Ohio State University, Ph.D., 1972
Engineering, metallurgy

University Microfilms, A XEROX Company, Ann Arbor, Michigan

© Copyright by

David Winfield Short

1972

THIS DISSERTATION HAS BEEN MICROFILMED EXACTLY AS RECEIVED.

THE INFLUENCE OF SURFACE CHARGE AND SURFACE STRUCTURE ON THE SUBLIMATION OF IONIC CRYSTALS

DISSERTATION

Presented in Partial Fulfillment of the Requirements for the Degree Doctor of Philosophy in the Graduate School of The Ohio State University

By

David Winfield Short, B.S. Met. E.

* * * * *

The Ohio State University
1972

Approved by

J. P. Hirth

Robert A. Rapp

Advisers
Department of Metallurgical Engineering

PLEASE NOTE:

Some pages may have

indistinct print.

Filmed as received.

University Microfilms, A Xerox Education Company

DEDICATION

To my wife Cheryl, whose love, patience, and encouragement helped make this work possible.

ACKNOWLEDGEMENTS

I am happy to acknowledge the support of this work by the U.S. Office of Naval Research under Contract N00014-67-023209995. The generous aid given by the National Aeronautics and Space Administration and the Kennecott Copper Company is also appreciated. I wish to thank Bud Farrar for his help in using the scanning electron microscope and Peter Whibley for his suggestions and aid in the construction of the experimental system. I especially wish to thank Professors John P. Hirth and Robert A. Rapp, my advisers, whose continuous intellectual inspiration and kindly guidance have made this work possible.

VITA

January 28, 1945	Born - Ashland, Kentucky
1967	B.S. Met. E., The University of Pennsylvania, Philadelphia, Pennsylvania
1967-1970. . . .	N.A.S.A. Trainee, Department of Metallurgical Engineering, The Ohio State University, Columbus, Ohio
1970-1971. . . .	Kennecott Fellow, Department of Metallurgical Engineering, The Ohio State University, Columbus, Ohio
1971-1972. . . .	Research Associate, Department of Metallurgical Engineering, The Ohio State University, Columbus, Ohio

PUBLICATIONS

H. Kressel, D. W. Short, and N. Brown, "The Electrical Resistivity Recovery of Cold-Worked High Purity Nickel," Acta Met. 15, 525(1967).

R. L. Heestand, D. W. Short, and W. H. Robinson, "Chemical Vapor Deposition of Ceramic Compounds," in Chemical Vapor Deposition of Refractory Metals, Alloys, and Compounds, edited by A. C. Schaffhauser (American Nuclear Society, Inc., Hinsdale, Illinois, 1967), pp. 175-191.

D. W. Short, R. A. Rapp, and J. P. Hirth, "The Influence of Surface Charge and Surface Structure on the Sublimation of Ionic Crystals," J. Chem. Phys. (accepted).

FIELDS OF STUDY

Major Field: Metallurgical Engineering

Studies in Evaporation. Professors John P. Hirth and Robert A. Rapp

CONTENTS

Page

DEDICATION ii

ACKNOWLEDGEMENTS iii

VITA iv

TABLES vi

FIGURES. vii

Chapter

I. INTRODUCTION 1

II. THEORETICAL DEVELOPMENT. 9

A. Calculation of the Distribution Potential
B. Relationship Between Surface Charge and Surface Structure
C. Discussion

III. EXPERIMENTAL APPARATUS AND PROCEDURE 50

A. Experimental Apparatus
B. Zirconia Oxygen Pump
C. Sample Preparation
D. Experimental Procedure
E. Surface Morphology

IV. RESULTS AND DISCUSSION 77

A. Results of Sublimation Experiments
B. Discussion of Results
C. Suggestions for Future Work

V. SUMMARY AND CONCLUSIONS. 101

APPENDIX

A 103

B 109

REFERENCES 114

TABLES

Table		Page
1.	Binding Energies for Particles on the Surface of NaCl at 900°K	15
2.	Sublimation Results for Several II-VI Compounds	39
3.	Zinc Oxide (ZnO) Crystals as Purchased from 3M Co., Typical Analysis	69
4.	Sublimation of Zinc Oxide in Argon-Oxygen Mixture	79
5.	Sublimation Conditions for Thought Experiment	90

FIGURES

Figure		Page
1.	Schematic view of crystal-gas interface, showing ledges and atomic position. Site a is in the crystal, b is in ledge, c is a kink, d is at ledge, and e is adsorbed on the surface.	5
2.	Defect formation processes for a sodium vacancy, V'_{Na}, and a chlorine vacancy, $V_{Cl}^{\cdot}$	10
3.	Geometric kinks as defined in terms of the attached coordinate system. Positions a, b and c are positive geometric kinks and d, e, and f are negative geometric kinks	25
4.	A hard sphere model of ZnO illustrating a double kink on the $(000\bar{1})$ oxygen surface. Dark spheres represent zinc ions and white spheres represent oxygen ions	26
5.	Another double kink on the $(000\bar{1})$ surface of ZnO which differs geometrically from that shown in Fig. 3	27
6.	The $(000\bar{1})$ surface with an oxygen ion removed from the kink position on left, exposing zinc ion	28
7.	A hard sphere model of ZnO illustrating a double kink on the (0001) zinc surface	30
8.	The double kink in Fig. 7 with a zinc ion removed from the kink position on the right.	31
9.	The evaporation rates of cadmium-doped CdS single crystal c faces a function of time at T = 730°C	44
10.	Evaporation rate of the (0001) face of CdS at 715°C while copper diffuses into the crystal from the (0001) face . .	47
11.	The evaporation rate of CdS single-crystal c face as functions of sulfur and cadmium impingement rates..	48
12.	Schematic illustration of experimental system.	52
13.	Crystal support.	54

FIGURES (Continued)

Figure		Page
14.	Alumina crystal holder	55
15.	Zirconia oxygen pump	58
16.	Characteristics of zirconia pump	65
17.	Zinc surface of chemically etched zinc oxide single crystal (500x, optical, 90 sec. 20 volume % nitric acid).	71
18.	Oxygen surface of chemically etched zinc oxide single crystal (500x, optical, 90 sec. 20 volume % nitric acid).	72
19.	Zinc surface of chemically etched zinc oxide single crystal (1000x, SEM at 49° tilt, 90 sec. 20 volume % nitric acid).	73
20.	Oxygen surface of chemically etched zinc oxide single crystal (1000x, SEM at 45° tilt, 90 sec. 20 volume % nitric acid).	74
21.	Sublimation rate of zinc oxide single crystal c-faces as function of oxygen partial pressure at ~1100°C	78
22.	Zinc surface of zinc oxide crystal after sublimation at ~1100°C and ~10^{-13} atm. O_2 (1000x, SEM at 45° tilt).	81
23.	Zinc surface of zinc oxide crystal after sublimation at ~1100°C and ~10^{-2} atm. O_2 (1000x, SEM at 45° tilt).	82
24.	Shielded zinc surface of zinc oxide after sublimation of oxygen surface showing peak formation (1000x, SEM at 45° tilt)	83
25.	Zinc surface of contaminated zinc oxide crystal showing peaks formed after sublimation at ~1100°C and ~10^{-10} atm. O_2 (1000x, SEM at 45°tilt).	84
26.	Oxygen surface of zinc oxide single crystal after sublimation at ~1100°C and ~10^{-13} atm. O_2 (1000x, SEM at 49° tilt)	85
27.	Oxygen surface of zinc oxide single crystal after sublimation at ~1100°C and ~10^{-10} atm. O_2 (1000x, SEM at 45° tilt)	86
28.	Oxygen surface of zinc oxide single crystal after sublimation at ~1100°C and ~10^{-2} atm. O_2 (1000x, SEM at 45° tilt)	87

FIGURES (Continued)

Figure		Page
29.	The evaporation rate of CdS single-crystal c face as functions of sulfur and cadmium impingement rates	96
30.	The distribution and geometry of point charges assumed to represent the charged defect distribution	104

INTRODUCTION

Since present and future technology may require substances with known and controlled physical properties such as sublimation and evaporation rates, it is important to know what factors affect these properties. The behavior of solids at high temperatures and in different environments has been a serious topic in industry, especially in the aerospace field. Although much experimental (empirical) data has been collected about the sublimation behaviour of metals and other solids, very little fundamental research has been carried out in order to determine the mechanisms which may act or control the sublimation behavior of ionic or near-ionic compounds. In light of this present situation, the few previous experimental studies of II-VI compounds have been reviewed and an extension of the multistep process theory has been developed and compared with experiment.

Numerous experimental and theoretical investigations of the vaporization of solids have appeared in the literature since the latter part of the nineteenth century. In 1882 Hertz[1] proposed that the maximum rate of vaporization, J_{max}, of a condensed phase can never exceed the rate at which atoms or molecules strike the surface under equilibrium conditions. Using kinetic theory, he showed that

$$J_{max} = nv/4 \qquad (1)$$

where n (molecules/cm^3) is the equilibrium vapor density and v (cm/sec)

is the mean speed of the molecules striking the surface. Later experiments by Knudsen[2] showed that impurities could reduce the predicted rate of vaporization by several orders of magnitude. By introducing a factor β, the condensation coefficient, into the right-hand side of equation (1) he accounted for the possibility that a fraction of the molecules striking the surface are reflected. This yields the classic Hertz-Knudsen expression,

$$J_c = \beta nv/4 \tag{2}$$

for condensation onto a surface. Substituting the appropriate expressions for the factors in equation (2) yields the more familiar form

$$J_c = \beta P_e /(2\pi mkT)^{1/2} \tag{3}$$

where P_e is the vapor pressure of the condensate at the absolute temperature T, m is the atomic mass, and k is Boltzmann's constant.

In Knudsen experiments, the effusion rate through an orifice of the specimen container is used to determine equilibrium vapor pressures. Normally β is assumed to equal unity (neglecting geometric and surface diffusion effect) for the temperatures at which measurements are made. These equilibrium studies yield thermodynamic data such as enthalpies and free energies of formation, but give only limited information about vaporization mechanisms. Hence, the evaporation rate from an equilibrium (Knudsen) cell is essentially determined by geometry and the thermodynamics of the system. In order to investigate the vaporization mechanism, experiments are usually performed under non-equilibrium conditions for which kinetics of vaporization are studied closely.

The study of the kinetics is usually accomplished by the Langmuir[3]-

type experiment in which the gross rate of vaporization, J, into a high vacuum is measured by the specimen weight loss. Kinetic measurements of this type are commonly referred to as "free evaporation" or "vacuum evaporation" experiments. It is usually assumed that J is independent of the vapor pressure of the condensed phase so that the measured flux is set equal to the flux under the equilibrium vapor pressure. From

$$J = \alpha P_e / (2\pi mkT)^{1/2} \qquad (4)$$

the equilibrium pressure may be calculated if α, the vaporization coefficent, is taken to be unity. However, quantitative comparisons of Langmuir and Knudsen experiments indicate that α may have values ranging from 10^{-6} to unity for monatomic solids (metals).[2,4-6] For these substances values of α largely different from unity are assumed to be caused by surface contamination.[7,8] For substances which vaporize as molecules or which dissociate during vaporization, the definition of α and the measurement of its departure from unity have not been established unequivocally.

In addition to the Langmuir technique, the kinetics of sublimation can be studied by vaporizing the solid in the presence of a foreign gas. This method is essentially a modification of the entrainment or transpiration technique. Analysis of these experiments is complicated by the diffusion of the gaseous molecules into the foreign gas, but valid information about mechanisms can be deduced under proper conditions. This method has been used for the experimental part of this investigation.

Since it is normally assumed that sublimation or vaporization is

a multistep process, atomic or molecular rearrangements may take place or a diffusion controlled reaction may occur on the vaporizing surface and precede the final desorption step. If the vaporization reactions, rearrangements, and subsequent processes occur consecutively, the particular process which is the slowest will determine the net sublimation rate.

In order to understand the behavior of atoms or molecules vaporizing from an arbitrarily oriented surface, a model is needed which corresponds to an equilibrium surface structure, yet can also be extended to vaporizing surfaces. Mechanistic theories based upon structural models should be useful to predict the relationship between positions and movements of surface atoms and the observed phenomena. The most commonly used model is based upon the anisotropy of interfacial surface energy discussed by Frank[9] and Cabrera[10]. Crystal surfaces are characterized as: (a) singular surfaces, being those for which grooved minima occur in a three-dimensional plot of surface energy versus orientation (usually coinciding with low index orientations); (b) vicinal surfaces, with orientations very close to those of singular surfaces and composed of low index planes separated by monomolecular/monoatomic ledges or steps; and (c) non-singular surfaces, being those which have interfacial free energies roughly independent of orientation.

A schematic representation of a vicinal surface showing the different atomic or molecular sites that can be occupied is shown in Fig. 1. The importance of ledges and kinks in the processes of vaporization and condensation were discussed in the late twenties by Kossel[11] and

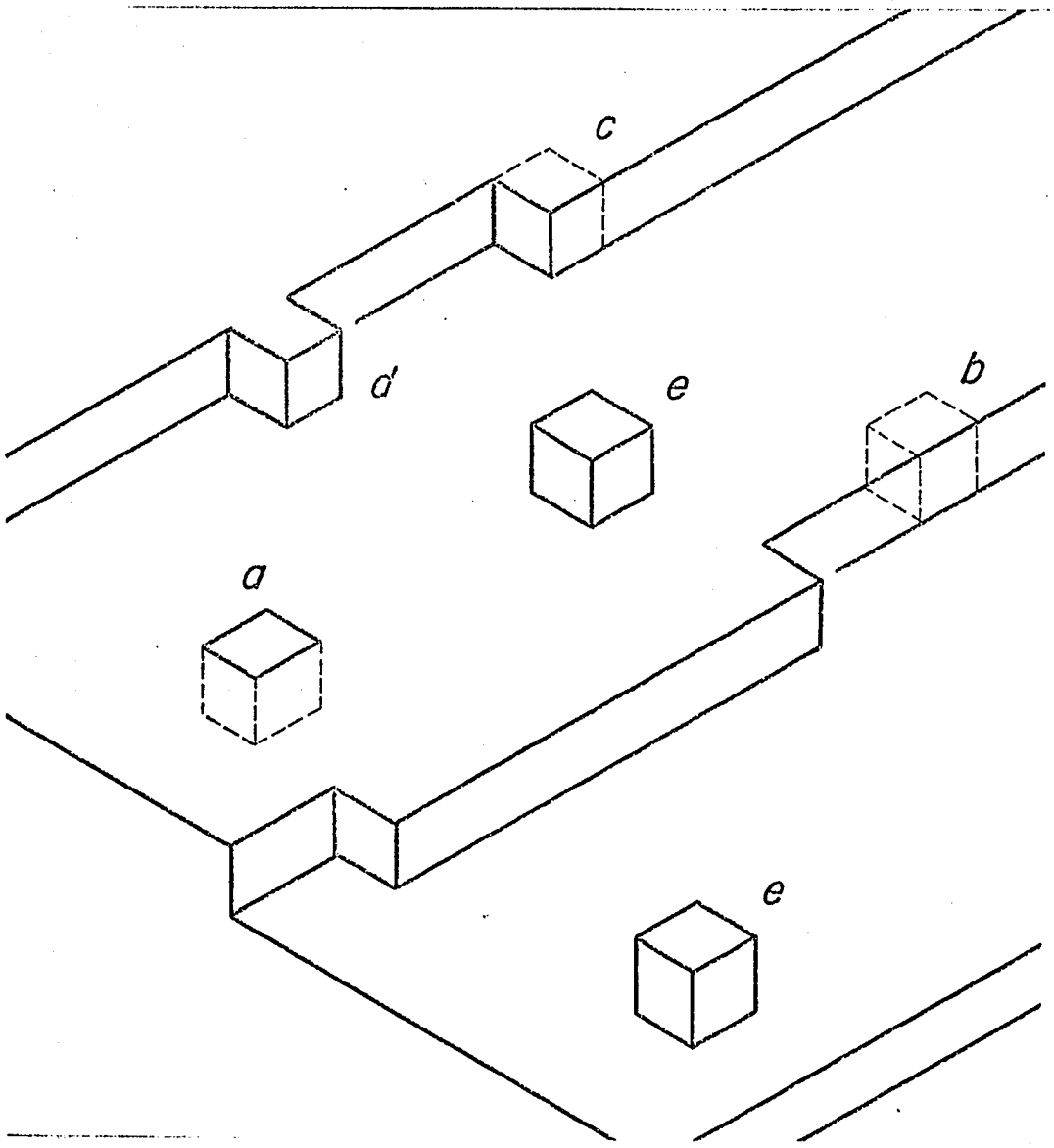

Figure 1: Schematic view of crystal-gas interface showing ledges and atomic position. Site a is in the crystal, b is in ledge, c is a kink, d is at ledge, and e is adsorbed on the surface.

Stranski.[12,13] Volmer[14] proposed a model for vaporization of solids which involved a multistep process in an attempt to explain the existing experimental evidence.[15,16] Following the theoretical development of the condensation process presented by Burton et al.,[17] the kinetics of vaporization by a ledge mechanism were treated by Knacke and Stranski[18] and Hirth and Pound[7].

This model is presently known as the terrace-ledge-kink (TLK) model of vaporization. Since crystal edges are favored sites for monomolecular ledge formation under vaporization, a perfect crystal bounded by singular surfaces may exhibit vicinal surfaces as the newly formed ledges move onto the singular surface.[8] For singular or vicinal surfaces the kinetics of vaporization may involve: (a) dissociation from kink sites to positions at ledges; (b) diffusion along the ledge; (c) dissociation from the ledge to an adsorbed position; (d) diffusion of the adsorbed atom or molecule along the surface; and (e) desorption from the surface to the vapor.

Using monoatomic ledge kinetics, Hirth and Pound[7] considered the possibility that surface diffusion of adatoms may limit the rate of vaporization. Following an absolute rate theory approach[19] to describe the kinetic importance of the different unit steps, the authors estimated values for the surface concentrations of the species. After estimating the relative values of the activation energies involved, the found that the net vaporization at equilibrium occurs predominantly by the dissociation of atoms from positions at ledges followed by desorption. The authors demonstrated that many pure metals vaporize with this dissocia-

tion-desorption process as the controlling step.

Observation of topological features formed during the sublimation or non-equilibrium vaporization of cadmium sulfide and zinc sulfide[20] and cadmium selenide[21] can be interpreted in terms of the TLK model of vaporization.[7,17,22] Munir and Hirth[20] suggest that the sublimation rate and surface morphology of certain II-VI compounds can be related to the existence of a charged defect distribution at the surface of AB type compounds. By analogy with the determination of the effective charges on crystal corners, edges and faces and on dislocation jogs, kinks on surface ledges of II-VI compounds can be shown to have effective charges of $\mp e$.[20,23] The surface charge, one-half of the charge distribution, manifests itself structurally as a difference in the concentrations of positively and negatively charged kink sites.

Frenkel first proposed the existence of a space-charge region near the surface of a pure ionic crystal in thermal equilibrium. Simply stated, for Frenkel defects, a charged surface and a space-charge region of the opposite sign arise because of the difference in the individual free energies of formation of a cation vacancy and a cation interstitial. Qualitatively, if the free energy to form the interstitial is more negative than that to form the vacancy, then at any finite temperature there is a tendency to form an excess of interstitial cations. Under these conditions, a positive space-charge region and a negative surface, i.e., the previously mentioned charged defect distribution, are formed and exist at thermal equilibrium. Lehovec[24], and later, Kliewer and Koehler[25] refined these early calculations to include

defect associations and impurity effects but only included the state of the surface implicitly in their developments. Poeppel and Blakely[26] then considered the separate energies involved in the creation of defects and showed that the results depended on the energy levels of the surface sites. The latter authors also investigated the binding states of surface ions and the density of the surfaces sites. However, they did not consider specific types of defect sites at surfaces.

In this paper, the surface defects are identified as surface kinks and detailed aspects of surface-bulk equilibrium are established for this case. Surface vacancies and adsorbed species represent alternative possibilities for surface defects on singular surfaces. Such entities can be treated by analogy to the kinks considered here, with identical results in terms of the concentrations of the appropriate surface defects. In addition, the earlier analyses[24-26] are extended to include surface-vapor equilibrium. More specifically, the charged defect distribution theory is developed mathematically and the concentrations of the charged kink sites and the strength of the dipole are related qualitatively to the observed vaporization behavior of several II-VI compounds.

THEORETICAL DEVELOPMENT

Calculation of the Distribution Potential

As a simple example we consider a sodium chloride single crystal with the Schottky-Wagner disorder, i.e., where charged sodium vacancies, V'_{Na}, and chlorine vacancies, $V^{\cdot}_{Cl}$, are the only defects present.[†] The defect formation processes are illustrated in Fig. 2. In sketch 2a, a cation vacancy is formed together with a kink of charge +e/2, while a kink with charge -e/2 is removed. In sketch 2b, the corresponding process is shown for an anion vacancy. Let ΔF^+ and ΔF^- be the free energies to form the charged sodium and chlorine vacancies, respectively, together with the formation and annihilation of the corresponding charged surface kinks. We note that ΔF^+ and ΔF^- have sometimes been called formation energies of vacancies alone;[24,25] but the associated defect must also be included in the analysis, whether it be a surface kink, an adsorbed ion, a surface vacancy, an electronic defect or an ion in the vapor phase. Also, while defect formation at a surface has been discussed previously,[24-26,28] the identification of a surface defect has not been made, leading to some confusion.[28] Suppose that ΔF^+ is

---

[†] According to the notation of Kroger and Vink,[27] V'_{Na} is a vacancy on a sodium site with a unit negative charge, -e, with respect to the normal site occupation; $V^{\cdot}_{Cl}$ is a vacancy on a chlorine site with a positive charge, +e, with respect to the normal site occupation.

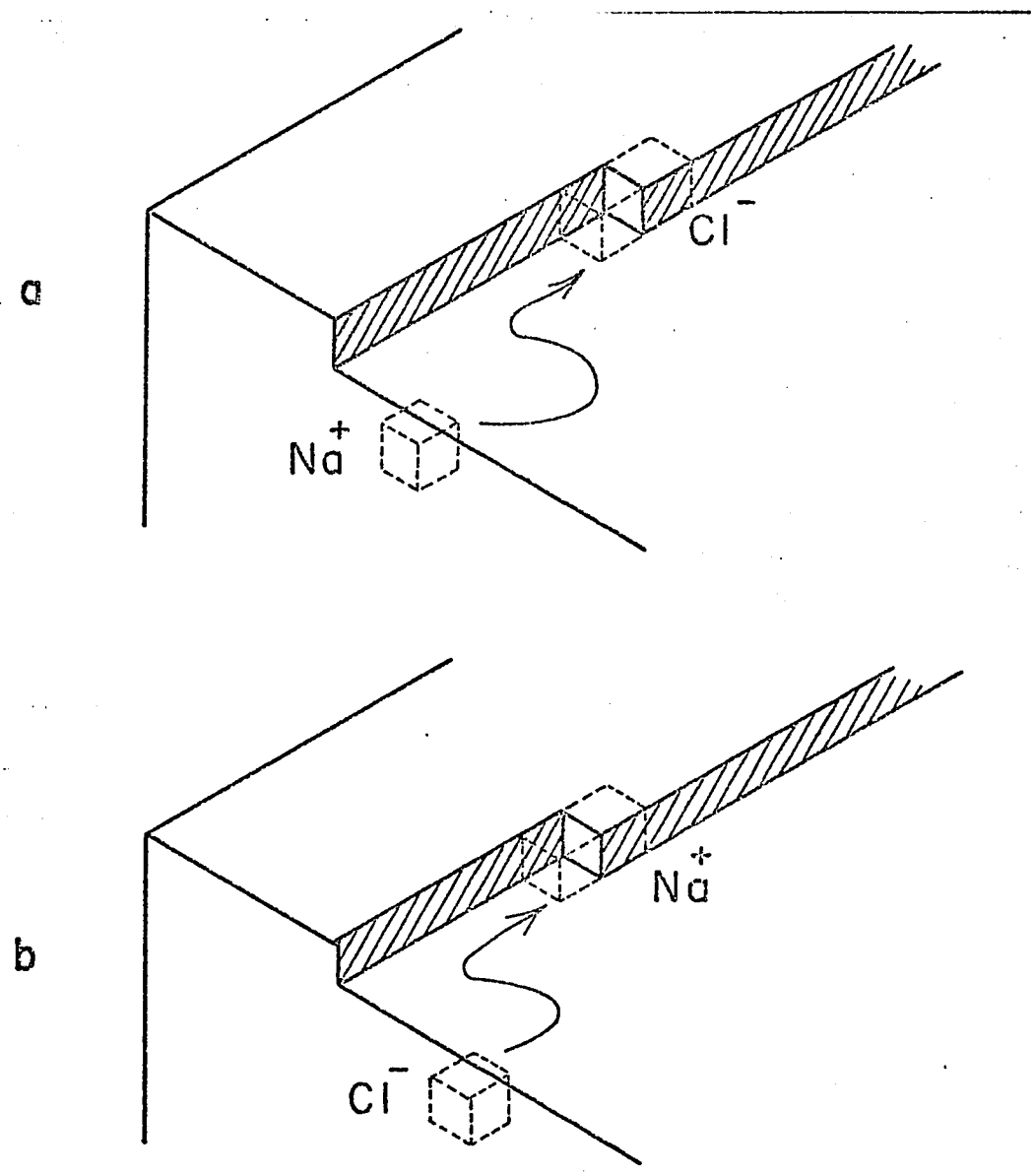

Figure 2: Defect formation processes for a sodium vacancy, V'_{Na}, and a chlorine vacancy, $V^{\bullet}_{Cl}$.

more negative than ΔF^-. Then, at any finite temperature a stoichiometric crystal has a tendency to form an excess of sodium vacancies resulting is a positive surface charge and a negative space-charge region within the crystal. At equilibrium there exists a Debye-Hückel dipole region with an associated potential difference, ϕ. For a sufficiently large neutral crystal, distributions from different surfaces do not interact and the effective free energy of defect formation is the energy to form the defect in the presence of the potential difference from a single surface. The model in such a case consists of an ideal crystal having infinite extent in the y and z directions, thus reducing the problem to a one-dimensional one.

The equilibrium defect concentrations in such a case are

$$[V'_{Na}](x) = N \exp -(\Delta F^+ - e\phi(x))/kT \qquad (5)$$

$$[V'_{Na}](x) = N \exp -(\Delta F^+ - e\phi(x))/kT \qquad (5)$$

$$[V^{\cdot}_{Cl}](x) = N \exp -(\Delta F^- + e\phi(x))/kT \qquad (6)$$

where $[V^{\cdot}_{Cl}]$ where $[V'_{Na}](x)$ is the local number of sodium vacancies per unit volume, N is $[V^{\cdot}_{Cl}](x)$ is the local number of chlorine vacancies per unit volume, and tion is assumed to be smooth enough to satisfy Poisson's equation for a medium with a static dielectric coefficient, κ. Therefore, Poisson's equation can be written as

$$\nabla^2\phi = -d^2\phi(x)/dx^2 = 4\pi\rho(x)/\kappa\epsilon_o \qquad (7)$$

where ϵ_o is the permittivity of vacuum and ρ is the charge per unit volume (the space charge), given by

$$\rho(x) = e([V^{\cdot}_{Cl}](x) - [V'_{Na}](x)) \qquad (8)$$

For this example only ionic defects are supposed to contribute to the space charge. The boundary conditions required for an analytical expression of the potential function are $\phi(0) = 0$ and $d\phi(\infty)/dx = 0$ for a semi-infinite crystal. The constant, asymptotic electric potential is found by the substitution of equations (5) and (6) into (8) with the additional condition that the space charge in the center of the crystal is zero. The result is

$$\phi(\infty) = (\Delta F^{+} - \Delta F^{-})/2e \qquad (9)$$

Equation (7) is solved by changing the parameters to the dimensionless variables $w(x) = (e/kT)[\phi(\infty) - \phi(x)]$ and $m = x/\lambda$ yielding

$$d^2w/dm^2 = 2\sinh(wP \qquad (10)$$

and

$$\lambda^2 = K\epsilon_o kT/4\pi e^2[V'_{Na}](\infty) \qquad (11)$$

The parameter λ is the Debye-Hückel distance. Note that λ is proportional to the square root of the equilibrium concentration (bulk concentration) of cation vacancies or anion vacancies since at $x = \infty$, their concentrations are equal at equilibrium. The solution of equation (7) as a function of the original parameter is found to be

$$\phi(x) = -(4kT/3)\tanh^{-1}(\exp(\sqrt{2x}/\lambda)\tanh(e\phi(x)/4kT)) + \phi(\infty) \qquad (12)$$

Equation (12) allows us to calculate the magnitude of the surface charge. By applying Gauss's Law,

$$\oint \underline{E}\cdot\underline{dA} = q/A, \qquad (13)$$

to the surface of the crystal, where $\underline{E}$ is the electric field intensity and $\underline{dA}$ is a unit of area, the charge per unit area can be calculated. The assumption made at this point is that the surface is a flat sheet

of charge. This assumption greatly simplifies calculation and provides adequate knowledge about the functional dependence of the surface charge layer. Moreover, for all but nearly singular surfaces, where the kink densities would be very low, the planar approximation should closely correspond to the actual charge. The planar model will also indicate qualitatively the behavior in the more complicated near-singular (vicinal) surface case.

The surface charge per unit area, Q, for this case is given by $Q = q/A = 2\epsilon_o E_n$ where $E_n = -(d\phi/dx)_{x=0}$ is the normal component of the electric field intensity exactly at the surface plane. For a crystal having a dielectric coefficient, K, the surface charge density is written

$$Q = -2K\epsilon_o(d\phi/dx)_{x=0}. \tag{14}$$

Equation (12) can be differentiated and substituted into equation (14) to give the dependence of the surface charge on the defect concentration,

$$Q = -8(2[V'_{Na}]\pi/K\epsilon_o kT)^{1/2} \sinh(e\phi(\infty)/2kT). \tag{15}$$

Evidently, the surface charge can influence the sublimation mechanism in three different steps: (a) desorption, (b) disconnection from ledges, and (c) a molecular combination process in the adsorbed layer.

In general, the desorption of a molecule having a natural dipole moment is treated as the removal of a dipole through the field of the charge distribution. The energy required to move the dipoles apart will depend on the magnitude and sign of the surface charge, the Deybe-Hückel distance, the orientation of the molecule with respect to

the surface of the crystal, and the orientation of the crystal. The energy to remove a sodium chloride molecule from a planar surface to infinity at 900°K is easily estimated. See Appendix A. The molecule is treated as a rigid dipole which is moved over a given distance to infinity while in the presence of the charged defect distribution. For the present considerations, the degree of hindered rotation of the molecule in the dipole field is sufficiently small that the rigid model is a valid approximation: the model can easily be extended to the hindered rotation case.[29] We assume the surface charge is distributed in a square grid of positive unit charges separated by a distance, d, where $d = (e/Q)^{1/2}$. A corresponding grid of negative unit charges is located in the crystal at a distance λ from the surface. The potential at any distance normal to the surface is the sum of the potentials due to the individual charges. We also assume that the dipole can approach the surface no closer than a chlorine ion diameter, 3.62Å. The actual distance of approach is uncertain since the position of the charge on a kink has not been identified. When calculating the potential by computer, we considered all the neighboring dipoles which contributed more than 10^{-6} volts to the total potential. This cutoff occurred with the three hundredth neighbor. Using for ΔF^+ and ΔF^- the values[25] $\Delta F^+ = 0.80$ eV-3.1kT and $\Delta F^- = 1.32$eV-3.1kT together with $N = 2.24 \times 10^{22}/cm^3$ and $\kappa = 5.62$, we find the energy to be approximately 0.25 eV.

The second case is one where the crystal sublimes with desorption of ions followed by combination in the vapor. In this case the energy to remove an ion from the surface is given by a simple potential

calculation and depends strongly upon all the previous factors except the orientation of the ion with respect to the surface. The energy to remove a chlorine ion at 900°K, calculated in a similar manner, is approximately 4.0 eV, which would preclude this process.

The last case is that of the desorption of a neutral atom. Here the dipole-dipole effect is small since the induced atomic dipole moment is very small. This energy is approximately 0.05 eV. Although the induced dipole moment is small here, it could possibly be large enough in certain systems to give a significant energy contribution.

Because the measured activation enthalpies of vaporization and enthalpies of sublimation for sodium chloride are approximately 2.7 eV and 2.3 eV,[30-32] respectively, the above calculations demonstrate that the total dipole-dipole interaction energy can be a significant part (15%) of the total sublimation energy.

Shown in Table 1 are calculated values of binding energies for the sodium chloride molecule, sodium ion, chlorine ion, sodium atom, and chlorine atom adsorbed on the surface of a crystal at 900°K.

TABLE 1. Binding Energies for Particles on the Surface of NaCl at 900°K

Particle	Distance, z	U(eV)	U(eV) for σ_{eff}
NaCl molecule	$2R_{Cl^-}+r_d$	-0.316	-0.222
NaCl molecule	$2R_{Cl^-}+r_d$	-0.380	-0.303
Cl ion	$2R_{Cl^-}$	-0.997	------
Na ion	$2R_{Na^+}$	+4.999	------
Cl atom	$2R_{Cl}$	-0.095	------
Na atom	$2R_{Na}$	-0.032	------

In all of the above situations, the dipole field near the surface of the crystal depends upon the atomic packing of the crystal. For symmetrically packed crystals like sodium chloride, the double layer dipole field is essentially the same for (100) surfaces as for $(\bar{1}00)$ surfaces. For crystals such as zinc sulfide, zinc oxide, cadmium sulfide, and others possessing the "wurzite" structure, the atomic packing leads to small surface dipoles on the (0001) and $(000\bar{1})$ surfaces[33,34] which are independent of the charged defect distribution and have opposite orientations with respect to a given coordinate system. This surface effect adds to or subtracts from the total field and should lead to a difference in observed sublimation rates from opposite c-axis faces. Any increase in Q will result in a decrease in the net rate of desorption.

The surface charge also can enter the sublimation mechanism during the disconnection of a particle from a ledge position. The analysis of the particle-distribution interaction is much more complex since the actual microscopic surface structure is difficult to describe. The value of the activation energy for an ion to move from a ledge position to the adsorbed position depends on the values of the surface charge, the Debye-Hückel distance, and the ledge spacing. The ledge spacing enters the mechanism since movement of a particle away from the ledge involves an additional energy contribution. This contribution arises from the slightly different direction of the local field intensity and the corresponding dipole-dipole interaction. The local field about a ledge will follow a Bessel function solution analogous

to that about a dislocation line[23]; however, it will smoothly merge into a planar field at distances from the surface equal to the ledge spacing. This is the basis for the earlier assertion that the quantitative planar model should apply closely to all but singular surfaces. As in the desorption situation, an increase in Q results in an increase in the energy for movement from a ledge to an adsorbed position. For molecules possessing permanent dipole moments, more complex ledge interactions can occur since reorientation of the molecule is possible in order to minimize the total energy. Hence, the charge Q influences ledge kinetics qualitatively in the same way as it influences the planar surface desorption kinetics.

Combination processes in the adsorbed layer can also be influenced by the presence of the Debye-Hückel distribution. If atoms or molecules must associate to sublime, the presence of the distributions field can restrict their motion. For example, an adsorbed sodium chloride molecule may have to diffuse over the surface and reorient itself with respect to the dipole field in order to form an adsorbed dimer. Changing its orientation would involve an energy change which would be dependent on the value of the distribution potential through the associated surface charge. Hence, the energy change is greater if the surface charge is larger. Thus an increase in the surface charge can reduc the rate of the combination process and then reduce the net sublimation rate.

Application of this theory to II-VI compounds is slightly more complex. The crystalline defects can consist of interstitial cations,

interstitial anions, cation vacancies, anion vacancies, compensating electrons and compensating holes. If the energies of formation for the defects were known, we could calculate all the concentrations and the actual surface charge subject to geometric considerations of surface morphology. Unfortunately, complete data of this nature is unavailable. Boswara and Franklin[35], in a recent review, discuss the theory used to calculate the energetics of simple defects in oxides. Most attempts to calculate individual vacancy formation energies in relatively simple alkaline earth oxides have been unsuccessful. Similar difficulty is expected for sulfides and selenides. Moreover, the use of the present models to characterize oxides which are more covalent, such as the IIA-VIA oxides, would be invalid. No attempt will be made in this paper to explain the theoretical method used to approximate the vacancy formation energies. The development of the charged defect distribution theory assumes that the individual defect formation energies will eventually be available.

Kröger[36] outlines a method similar to Lehovec's which allows interaction between a crystal and its environment. Two cases are examined: cadmium sulfide having the Schottky-Wagner disorder and zinc oxide having the Frenkel disorder. These are non-stoichiometric crystals and contain electronic defects in addition to those considered for the stoichiometric case of the preceding section. The consequences with respect to dipole formation, however, are the same as for the stoichiometric case.

Cadmium Sulfide

In pure cadmium sulfide, the disorder is of the Schottky-Wagner type. We assume that in the bulk or interior of the crystal four types of charged defects are present in appreciable amounts: vacant Cd sites, V'_{Cd}; vacant S sites, $V^{\cdot}_{S}$; electrons, e'; and holes, h$^{\cdot}$. A Kröger and Vink approach [27] can be taken to calculate the equilibrium concentrations of each of the defects in the interior of the crystal.

Assuming that the concentrations of vacancies, electrons and holes are so small in comparison with the number of lattice sites that their activities may be replaced by their concentrations (Henry's Law), we write six relations which define the concentrations of the defects:

1. Crystal-vapor equilibrium,

$$1/2\ S_2(g) \rightleftharpoons S_S^x + V_{Cd}^x, \text{ with } K_{S_2V} = [V_{Cd}^x]/P_{S_2}^{1/2} \qquad (16)$$

2. Native defect equilibrium,

$$0 \rightleftharpoons V_{Cd}^x + V_S^x, \text{ with } K_S = [V_{Cd}^x]\,[V_S^x] \qquad (17)$$

3. "Ionization" of the defect V_S^x,

$$V_S^x \rightleftharpoons V_S^{\cdot} + e', \text{ with } K_a = [V_S^{\cdot}]n/[V_S^x] \qquad (18)$$

4. "Ionization" of the defect V_{Cd}^x,

$$V_{Cd}^x \rightleftharpoons V'_{Cd} + h^{\cdot}, \text{ with } K_b = [V'_{Cd}]\,p/[V_{Cd}^x] \qquad (19)$$

5. Intrinsic defect equilibrium,

$$0 \rightleftharpoons e' + h^{\cdot}, \text{ with } K_i = np \qquad (20)$$

6. Electrical neutrality condition,

$$n + [V'_{Cd}] = p + [V_S^{\cdot}] \qquad (21)$$

Since there are six quations involving six unknown quantities, one can solve for their simultan s solutions. Each unknown concentration can be written as a function of the sulfur partial pressure and the given equilibrium constants. Conductivity experiments have shown that cadmium sulfide is an n-type semi-conductor leading to the assumption that the preponderant lattice defect is an ionized sulfur vacancy. The electrical neutrality condition simplifies to $n = [V_S^{\cdot}]$ if $n \gg [V_{Cd}^{'}]$ and $[V_S^{\cdot}] \gg p$. Solving equations (16)-(21) simultaneously in terms of the equilibrium constants and the sulfur partial pressure, we find expressions for the mole fractions of defects:

$$[V_{Cd}^{x}] = K_{S_2V} P_{S_2}^{1/2} \tag{22}$$

$$[V_S^{x}] = (K_S/K_{S_2V})\, P_{S_2}^{-1/2} \tag{23}$$

$$[V_{Cd}^{'}] = (K_b\, (K_{S_2V} K_S)^{1/2}/K_i)\, P_{S_2}^{1/4} \tag{24}$$

$$[V_S^{\cdot}] = (K_a K_S/K_{S_2V})^{1/2}\, P_{S_2}^{-1/4} \tag{25}$$

$$n = (K_a K_S/K_{S_2V})^{1/2}\, P_{S_2}^{-1/4} \tag{26}$$

$$p = K_i (K_{S_2V}/K_a K_S)^{1/2} P_{S_2}^{1/4} \tag{27}$$

Specifically the concentrations are in numbers of defects per unit volume.

Calculation of the Potential Function

The earlier reasoning leads to the expectation of an electrostatic potential, $\phi(x)$, which is zero at the surface and some constant value, $\phi(\infty)$, in the interior of the crystal. This potential would

enter into equations (22)-(29) in the following manner:

$$[V'_{Cd}](x) = \frac{K_b^o(K_{S_2V}^o K_S^o)}{K_i^o} P_{S_2}^{1/2} \exp\left(\frac{-U_{V'_{Cd}} + e\phi(x)}{RT}\right) \tag{28}$$

$$[V_S^{\cdot}](x) = \left(\frac{K_a^o K_S^o}{K_{S_2V}^o}\right)^{1/2} P_{S_2}^{-1/4} \exp\left(\frac{-U_{V_S^{\cdot}} - e\phi(x)}{kT}\right) \tag{29}$$

$$n(x) = \left(\frac{K_a^o K_S^o}{K_{S_2V}^o}\right)^{1/2} P_{S_2}^{-1/4} \exp\left(\frac{-U_{e'} + e\phi(x)}{kT}\right) \tag{30}$$

and

$$p(x) = K_i^o \left(\frac{K_{S_2V}^o}{K_a^o K_S^o}\right)^{1/2} P_{S_2}^{1/4} \exp\left(\frac{-U_h - e\phi(x)}{kT}\right) \tag{31}$$

where $U_{V'_{Cd}}$ and $U_{V_S^{\cdot}}$ are the energies, respectively, to remove a cadmium or sulfur ion from a particular position in the bulk phase and form positive or negative kinks on the surface; $U_{e'}$ and $U_{h^{\cdot}}$ are the energies, respectively, to form excess electrons or positive holes in the interior; the K^o's are the nominally temperature-independent, pre-exponential portions of the equilibrium constants K.

The charge density (coulombs per unit volume) at any position within the crystal can be written

$$\rho(x) = e\,([V_S^{\cdot}](x) - n(x) - [V'_{Cd}](x) + p(x)). \tag{32}$$

at $x = \infty$ equations (27)--(31) can be rearranged to give

$$V'_{Cd}(\infty)\exp\left(\frac{-e\phi(\infty)}{kT}\right) = K^*_{V'_{Cd}}\exp\left(\frac{-U_{V'_{Cd}}}{kT}\right)P_{S_2}^{1/4} \tag{33}$$

$$V^{\cdot}_{S}(\infty)\exp\left(\frac{e\phi(\infty)}{kT}\right) = K^*_{V^{\cdot}_{S}}\exp\left(\frac{-U_{V^{\cdot}_{S}}}{kT}\right)P_{S_2}^{-1/4} \tag{34}$$

$$n(\infty)\exp\left(\frac{-e\phi(\infty)}{kT}\right) = K^*_{e'}\exp\left(\frac{-U_{e'}}{kT}\right)P_{S_2}^{-1/4} \tag{35}$$

and=

$$p(\infty)\exp\left(\frac{e\phi(\infty)}{kT}\right) = K^*_{h^{\cdot}}\exp\left(\frac{-U_{h^{\cdot}}}{kT}\right)P_{S_2}^{1/4} \tag{36}$$

where the K*'s contain all the K^o's of equations (28)-(31). Upon substituting the expressions (33)---(36) into (32) we find the charge density written as a function of $\phi(x)$, $\phi(\infty)$, and the equilibrium concentrations of the defects in the form

$$\rho(x) = e\left\{\left[V^{\cdot}_{S}\right](\infty)\exp\left(\frac{e\phi(\infty)-e\phi(x)}{kT}\right) - \left[V'_{Cd}\right](\infty)\right.$$
$$\exp\left(\frac{-e\phi(\infty)+e\phi(x)}{kT}\right) - n(\infty)\exp\left(\frac{-e\phi(\infty)+e\phi(x)}{kT}\right) + p(\infty)$$
$$\left.\exp\left(\frac{e\phi(\infty)-e\phi(x)}{kT}\right)\right\} \tag{37}$$

Since the original electrical neutrality condition in the bulk of the crystal is, in number per unit volume,

$$\left[V'_{Cd}\right](\infty) + n(\infty) = \left[V^{\cdot}_{S}\right](\infty) + p(\infty), \tag{38}$$

equation (37) can be reduced to

$$\rho(x) = e\left\{[V_S^{\cdot}](\infty) + p(\infty)\right\}\left\{\exp\left(\frac{e\phi(\infty)-e\phi(x)}{kT}\right) - \exp\left(\frac{-e\phi(\infty)+e\phi(x)}{kT}\right)\right\} \tag{39}$$

Note that either side of equation (38) can be used to generate equation (39). By defining $w(x) = (e/kT)\,(\phi(\infty) - \phi(x)) < 0$ and substituting it into equation (39), we find the charge density to be

$$\rho(w) = 2e\,([V_S^{\cdot}](\infty) + p(\infty))\sinh(w) \quad . \tag{40}$$

Inspection of equation (40) shows that it has the same functional form as equation (10). Therefore, the solution of equation (7) for the non-stoichiometric CdS crystal will be identical except for the value of $\phi(\infty)$ and λ. The functional dependence of the surface charge on the sum of the equilibrium defect concentrations is analogous to that given by equation (15),

$$Q = -8\,([V_S^{\cdot}](\infty) + p(\infty))^{1/2}\,(2\pi\epsilon\epsilon_o kT)^{1/2}\,\sinh\frac{e\phi(\infty)}{2kT} \tag{41}$$

ZnO

Zinc oxide is usually assumed to possess a Frenkel type disorder, with interstitial zinc, $Zn_i^{\cdot}$, and zinc vacancies, V_{Zn}', being the preponderant ionic defects.[27] Equations analogous to (16)-(40) can also be written to describe this II-VI compound. The electrical neutrality condition for ZnO takes the form:

$$[Zn_i^{\cdot}](\infty) + p(\infty) = [V_{Zn}'](\infty) + n(\infty). \tag{42}$$

As in the CdS case, either side of equation (42) can be used in the expression for the ZnO space charge. The substitution of the left-hand-

side of equation (42) into equation (40) yields

$$\rho(w) = 2e\left([Zn_i^{\cdot}](\infty) + p(\infty)\right) \sinh(w). \qquad (43)$$

The solution of Poisson's equation is exactly the same as presented previously. The surface charge for a zinc oxide crystal is given by

$$Q = -8\left([Zn_i^{\cdot}](\infty) + p(\infty)\right)^{1/2} (2\pi\epsilon\epsilon_0 kT)^{1/2} \sinh\frac{e\phi(\infty)}{2kT}. \qquad (44)$$

Relationship Between Surface Charge and Surface Structure

Given that an ionic crystal in equilibrium possesses a surface charge, the problem remains to relate this surface charge to the microscopic surface structure, i.e., the relative concentrations of positively charged and negatively charged kink positions with charge $\pm$ q.

Viewing a packing model of a typical II-VI compound, ZnO, we find four different geometric kink structures on the $(000\bar{1})$ plane and four different structures on the (0001) plane. Shown in Figure 3 is a sketch in which the negative and positive geometric kink sites are defined in relation to a given coordinate system. When viewed along the ledge in a positive y direction a positive kink position is defined as a site where the ledge advances in the positive x direction. A negative kink position is defined by an advance in the negative x direction. Figures 4 and 5 illustrate the four different geometric kink structures found on the $(000\bar{1})$ oxygen surface in zinc oxide. Let us examine a double kink of the form in Figure 5 with an oxygen ion at the left positive kink position. Removing this oxygen ion to the vapor, as shown in Figure 6, removes a -2e charge and leaves the double kink with a net positive charge, q. A comparison of the geometrically positive

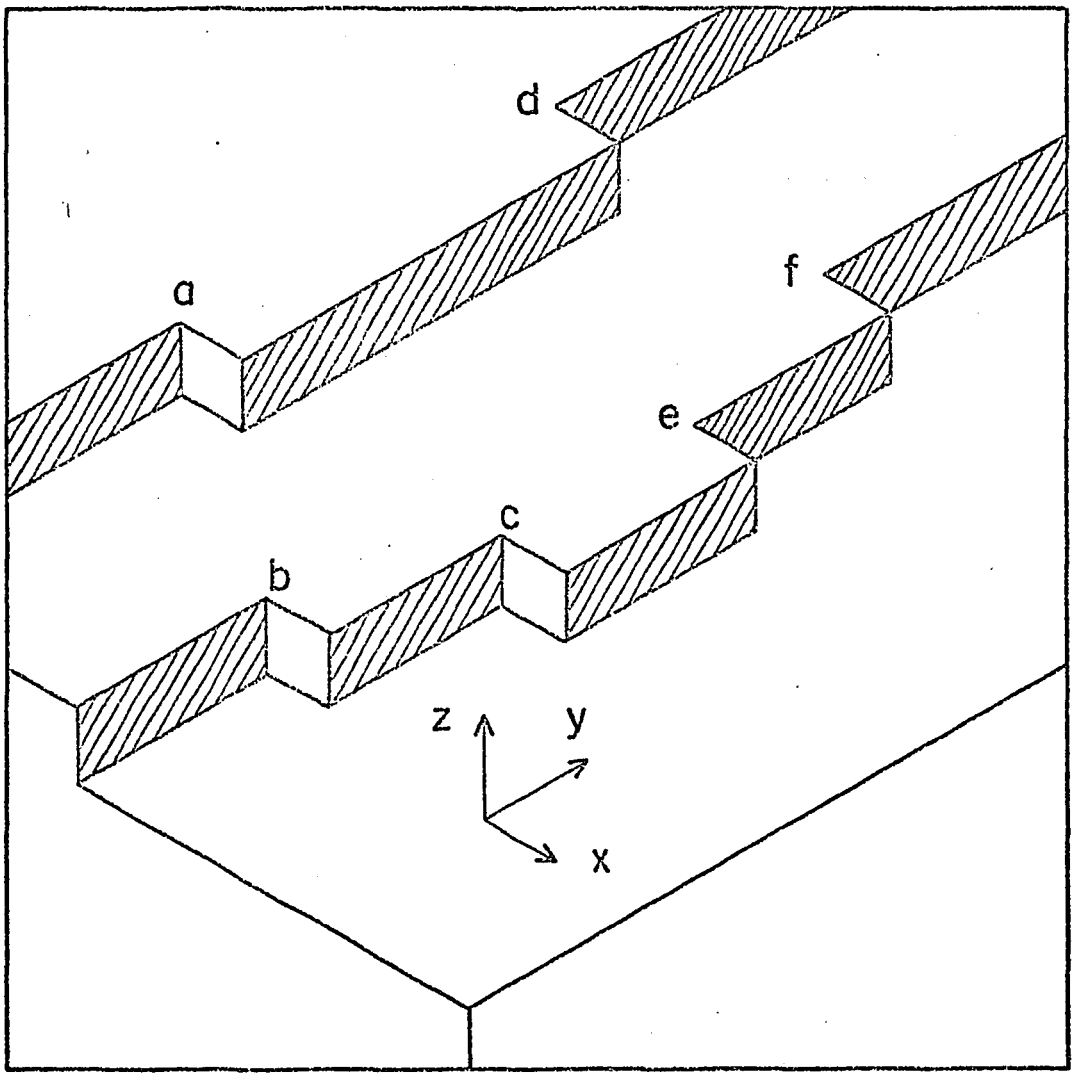

Figure 3: Geometric kinks as defined in terms of the attached coordinate system. Position a, b and c are positive geometric kinks and d, e and f are negative geometric kinks.

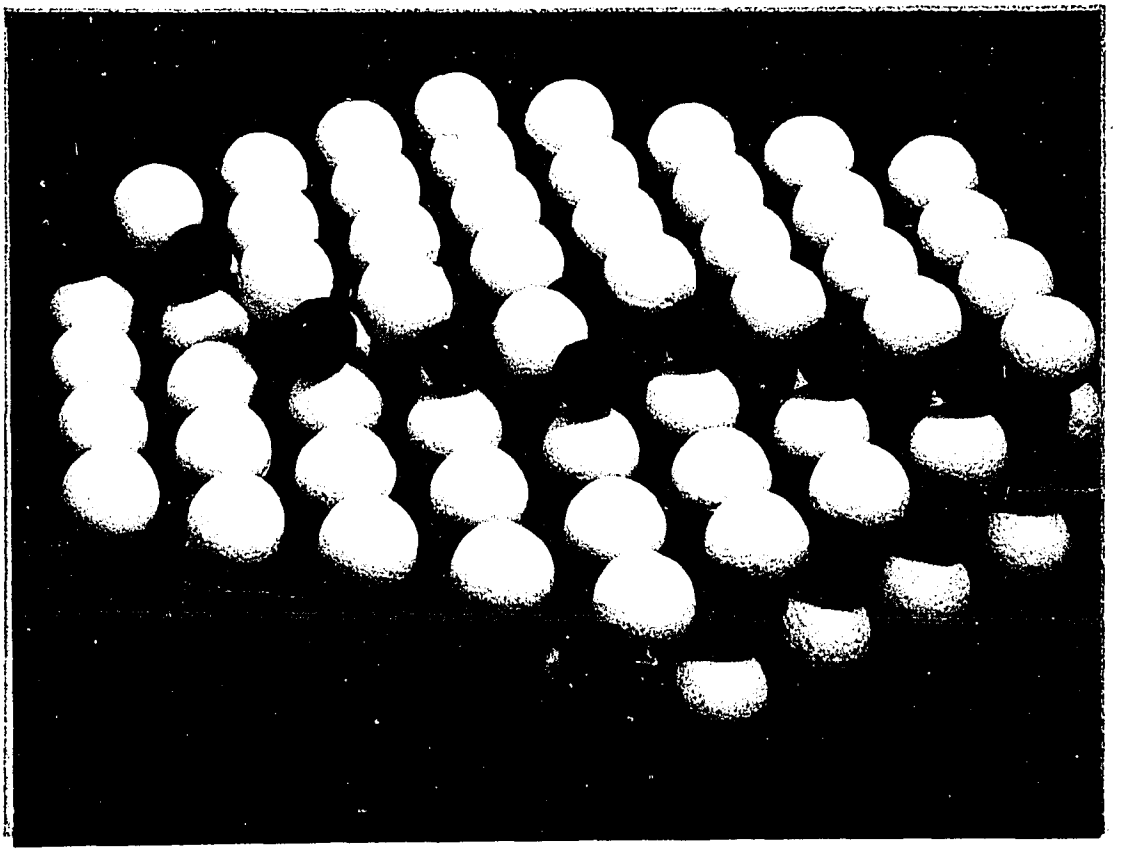

Figure 4: A hard sphere model of ZnO illustrating a double kink on the (0001) oxygen surface. Dark spheres represent zinc ions and white spheres represent oxygen ions.

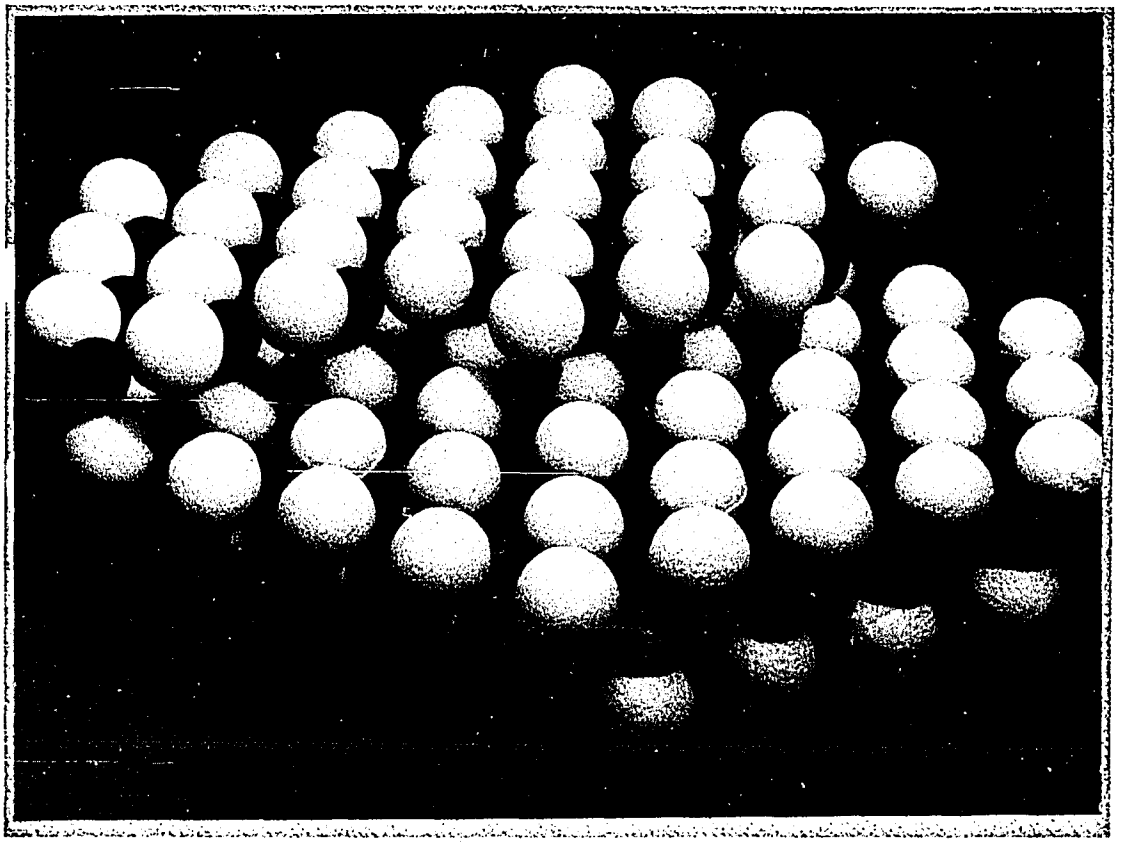

Figure 5: Another double kink on the $(000\bar{1})$ surface of ZnO which differs geometrically from that shown in Figure 3.

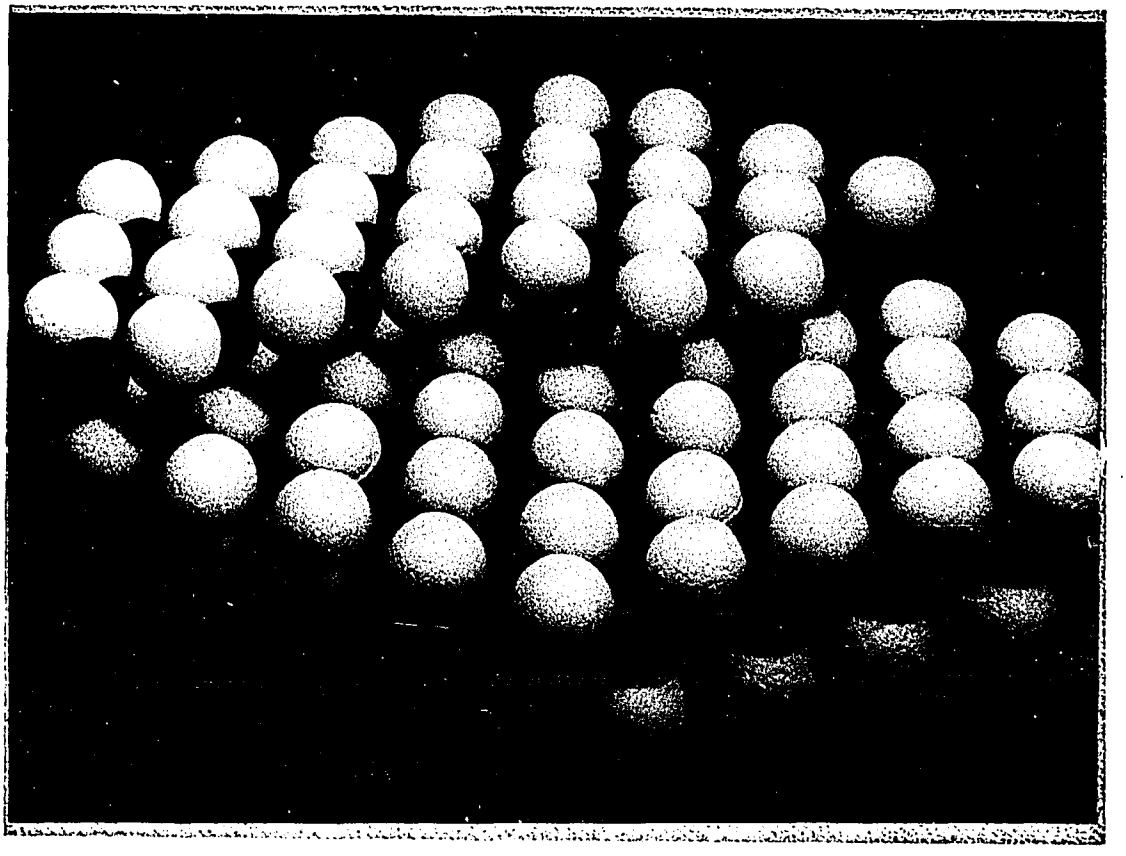

Figure 6: The $(000\bar{1})$ surface with an oxygen ion removed from the kink position on left, exposing zinc ion.

kink without the oxygen ion in Figure 6 and the geometrically negative kink in Figure 5 shows that they are mirror images. Charge balance requires that $\underline{q}-(-2e) = -\underline{q}$ or $\underline{q} = -e$ for the structure examined. Figure 7 shows a double kink on the (0001) Zn surface. Removing the Zn ion from the right kink site to the vapor, as shown in Figure 8, removes a +2e charge and leaves the double kink with a net negative charge. A comparison of the two structures in Figure 8 shows that they are also mirror images. Charge balance here requires $\underline{q} - 2e = -\underline{q}$ or $\underline{q} = e$. Other kink structures can be inspected with similar results, showing that the local charge at a kink site is $\pm$ e.

If one defines X^+ as the average number of cations in a kink position per unit length of ledge and X^- as the average number of anions in a kink position per unit length of ledge, the surface charge density can be written as

$$Q = e\ (X^+ - X^-)\ L \tag{45}$$

where L is the ledge length per unit surface area. Another equation is needed to solve for the magnitudes of X^+ and X^-:

A method for finding this second relation between X^+ and X^- is suggested by Hirth and Lothe.[23] The authors show how the equilibrium concentration of kinks is directly related to their free energy of formation. A similar approach is taken here. One simply minimizes the total free energy per unit ledge length, F, with respect to a change in the number of double kinks, N_{pr}, as derived in Appendix B. The final expressions relating the concentration of positively charged and negatively charged kinks to the surface charge are derived in Appendix B

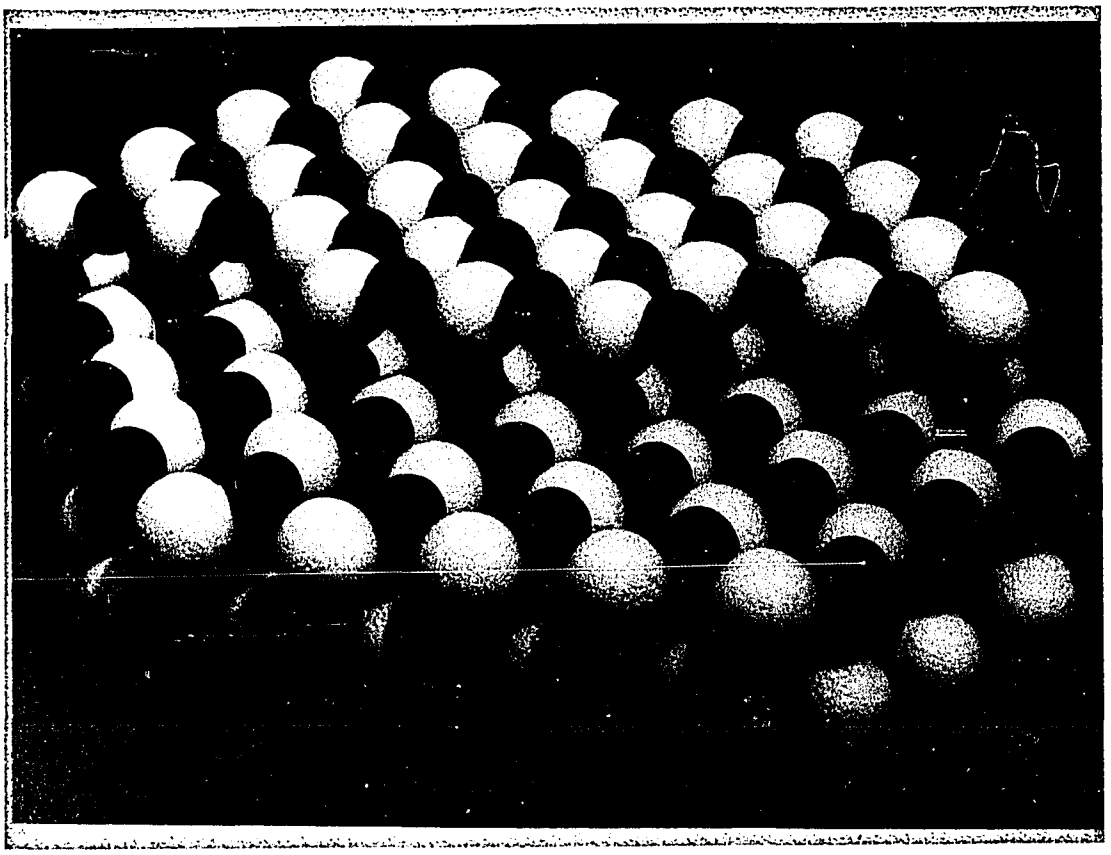

Figure 7: A hard sphere model of ZnO illustrating a double kink on the (0001) zinc surface.

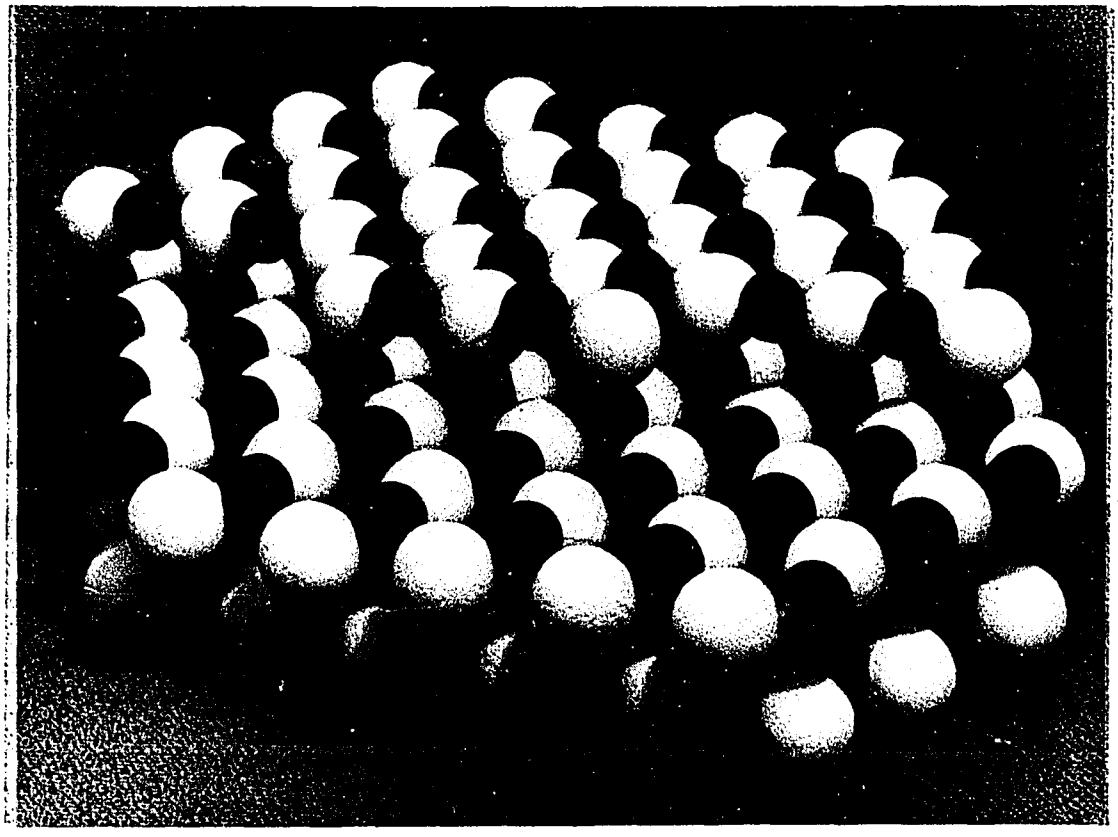

Figure 8: The double kink in Figure 7 with a zinc ion removed from the kink position on the right.

and are given by:

$$X^+ X^- = 4 \exp\left(\frac{-2U_k}{kT}\right) \tag{46}$$

or

$$X^+ \left(X^+ - \frac{Q}{e L}\right) = 4 \exp\left(\frac{-2U_k}{kT}\right) \tag{47}$$

and

$$X^- \left(X^- + \frac{Q}{e L}\right) = 4 \exp\left(\frac{-2U_k}{kT}\right) \tag{48}$$

where U_k is the kink formation energy.

Since the kinks and point defects are thermally activated, X^+ and X^- should asymptotically approach zero as the temperature, T, approaches zero. Although this result is not readily evident in equations (47) and (48) and it is the case since Q also approaches zero as T approaches zero. These limiting conditions are consistent with general entropy considerations. Moreover, analogous to the result of Poeppel and Blakely[26], the influence of surface orientation on the sublimation rate is given by the parameter L, the total length of ledge per unit area.

Discussion

Theoretical Analysis

The value of the defect distribution potential and its associated field will depend upon the magnitude of the surface charge density, Q. If one postulates that during the sublimation of a particular species, work is required to overcome the dipole-particle attraction, then the

total energy required to remove particles from the solid to the vapor also will depend upon the magnitude of the surface charge density in the manner discussed previously. If Q is decreased, the sublimation energy is decreased. This should yield an increase in the net sublimation rate.

If dissociation from a kink is the controlling mechanism in the consecutive sublimation steps, any change in the kink concentration will also affect the net rate.[8,22] Since with all other factors remaining constant, any increase in Q results in an increase in either X^+ or X^- through equations (47) and (48), and there should be a decrease in the net rate. Also as discussed in the section on the potential value, an increase in Q could increase the activation energy of the disconnection from the kink step of the process, and this would also decrease the net sublimation rate. Thus, a change in any parameter which tends to increase the surface charge density should decrease the net sublimation rate. Observations of the sublimation behavior of several II-VI compounds now are discussed in terms of these predictions.

In the following analysis of cadmium sulfide sublimation experiments, atomic packing and the effects of doping and illumination on the equilibrium concentrations of ionic and electronic defects are considered in relation to the double layer dipole theory.

If the crystal is in equilibrium with a gaseous environment, one reaction describing the state may be written as

$$1/2\ S_2(g) + V_S^{\cdot} + e' \rightleftharpoons S_S^{x} \qquad (49)$$

with a corresponding relation between the reactants and products

given by

$$[V_S^{\cdot}]\, n = K_1\, P_{S_2}^{-1/2} \quad . \tag{50}$$

For the pure CdS crystal at sufficiently high P_{S_2}, where electrons and sulfur vacancies are the preponderant defects the electrical neutrality condition can be approximated as

$$n = [V_S^{\cdot}] \quad . \tag{51}$$

For the pure CdS crystal, the calculated concentrations of electrons, n, and vacancies, $[V_S^{\cdot}]$, result from the substitution of equation (51) in to equation (50) which yields

$$[V_S^{\cdot}] = n = K_1^{1/2}\, P_{S_2}^{-1/4} \quad . \tag{52}$$

For a copper-doped CdS crystal at sufficiently high P_{S_2}, the simplified neutrality condition can be written as

$$[Cu'_{Cd}] + n = [V_S^{\cdot}] \quad . \tag{53}$$

As the concentration of copper increases in the crystal, the electron concentration is reduced until eventually the sulfur vacancy concentration equals the copper concentration, i.e.

$$[Cu'_{Cd}] = [V_S^{\cdot}] \quad . \tag{54}$$

We can write an equation showing the effective ionization of a copper atom as it goes into a substitutional position in the lattice as

$$Cu(s) \rightleftharpoons Cu'_{Cd} + V_S^{\cdot} \tag{55}$$

Its corresponding concentration expression is

$$[Cu'_{Cd}][V^{\cdot}_{S}] = K_2 a_{Cu} = K_3 \tag{56}$$

where A_{Cu} is the activity of copper. After substituting equation (56) into equation (53) and solving the quadratic equation, we have the general expression for the sulfur vacancy concentration,

$$[V^{\cdot}_{S}] = \frac{n}{2} + \left(\frac{n^2}{2} + 4K_3\right)^{1/2} . \tag{57}$$

For the pure CdS crystal where $n^2 \gg 4K_3$, i.e., a very small concentration of Cu is in the lattice, equation (57) reduces to equation (51) and (52). For the very slight Cu doping where $4K_3 \gg n^2$, equation (57) yields

$$[V^{\cdot}_{S}] = K_3^{1/2} = (K_2 a_{Cu})^{1/2} \tag{58}$$

and

$$n = K_1 (K_3 P_{S_2})^{1/2} \tag{59}$$

which are the same results obtained from the direct combination of equations (50), (54), and (56). Equations (58) and (59) show that for a heavily doped crystal, the concentration of charged sulfur vacancies is a function only of the temperature and the copper activity. The concentration of electrons is inversely proportional to the square root of the sulfur partial pressure and the copper activity. Kröger, Vink, and Van den Boomgaard[37] assume that this explanation, i.e., that of vacancy creation, holds for the incorporation of silver in cadmium sulfide and suggest that copper behaves similarily.

An alternate reaction involving copper as a dopant is the displacement of some cadmium by the dopant, resulting in the precipitation of cadmium and corresponding to an increase in the cadmium activity. This reaction can be written

$$Cu(s) + Cd^{x}_{Cd} + e' \rightleftharpoons Cd(s) + Cu'_{Cd} , \tag{60}$$

with the equilibrium concentration of substitutionally added copper given by

$$[Cu'_{Cd}] = K_4 n \, (a_{Cu}/a_{Cd}) = K_5 n. \tag{61}$$

After substituting equation (61) into equation (53) we obtain

$$[V_S^{\cdot}] = n \, (1 + K_5). \tag{62}$$

The sulfur pressure relationships for $[V_S^{\cdot}]$ and n are found by combining the last equation with equation (50); thus,

$$[V_S^{\cdot}] = K_1^{1/2} \, (1 + K_5)^{1/2} \, P_{S_2}^{-1/4} \tag{63}$$

and

$$n = (K_1^{1/2}/(1 + K_5))^{1/2} \, P_{S_2}^{-1/4} \tag{64}$$

Whether the vacancy creation or the cadmium displacement explanation is accepted as the actual mechanism, the equations yield an increase in the charged sulfur vacancy concentration and a decrease in the electron concentration when the copper is incorporated into the crystal.

When a pure CdS crystal is illuminated with light of energy greater than the band gap, both holes and electrons of equal concentrations are produced, i.e. both n and p increase.[38] At sufficiently high P_{S_2},

this light effect tends to increase the value of n in equation (50) and thereby decreases the charged sulfur vacancy concentration. At the same time, the increase in the hole concentration can yield an annihilation of the charged cadmium vacancies which are only a negligible fraction of the total number of defects.

For the copper-doped case, where initially the electron concentration is small and the sulfur vacancy concentration is large, illumination causes an increase in the former and a decrease in the latter. Both changes, however, are negligible when compared to their original, non-illuminated concentrations. The resulting increase in the electron concentration also could be associated with the precipitation of cadmium metal in the crystal.[39]

In summary, the following effects are expected:

1. Changing the stoichiometry of CdS toward a more sulfur-rich composition decreases both $[V_S^{\cdot}]$ and n.

2. Changing the stoichiometry of CdS toward a less sulfur-rich composition, by adding cadmium or lowering the P_{S_2} increases both $[V_S^{\cdot}]$ and n.

3. Doping with copper decreases n and increases $[V_S^{\cdot}]$.

4. Illumination with radiation greater than the bank gap energy for the pure CdS increases n and decreases $[V_S^{\cdot}]$.

5. For the copper-doped crystal where initially n is small and $[V_S^{\cdot}]$ is large, appropriate illumination causes an increase in n, to a value still small compared to the undoped case, and a decrease in $[V_S^{\cdot}]$.

Cadmium could also be precipitated.

Comparison with Experiment

A number of experiments have been performed on the sublimation of II-VI compounds as summarized in Table 2. These results are discussed individually and compared with the preceding section below.

Somorjai and Jepsen[40] reported that the basal faces of cadmium sulfide single crystals vaporize in vacuum with a rate approximately one tenth the value of the gross equilibrium rate. Leonard[41] confirmed this observation and also reported that the cadmium face, (0001), vaporized with a rate approximately 30% faster than the sulfur face, $(000\bar{1})$. From his scanning electron microscope photographs, he showed that the sulfur face seems to have the larger area, negating the possibility that the observed rates are due to a simple area difference. Observations of topological features by Munir and Hirth[20], and Munir, et at.[21], different enthalpies of vaporization measured by Leonard,[41] and differences in surface morphology evident in all the experiments suggest a definite link between the surface structure and the mechanism of vaporization.

The asymmetry in the free evaporation rates of cadmium sulfide single crystals reported by Leonard,[41] is expected if the surface charge is considered to have a significant effect. According to the theory proposed here, the presence of positively charged sulfur vacancies near the surface of the crystal creates a Debye-Hückel distribution with a negative orientation, i.e., the surface possesses a negative charge with respect to the underlying space charge. The asymmetrical behavior

TABLE 2: Sublimation Results for Several II-VI Compounds

Single Crystal Conditions	Observations	References
Pure CdS, Vacuum Sublimation	$J^{net}_{normal} / J^{net}_{equilibrium} \cong 0.1$	40
	$J^{net}_{(0001)\ Cd\ face} \cong 1.3\ J^{net}_{(000\bar{1}),\ O\ face}$	41
S-doped CdS, vacuum sublimation	$J^{net}_{S\ doped} < J^{net}_{normal}$	45
s-doped CdS, irradiated ($h\nu > Egap$), vacuum sublimation	$J^{net}_{irradiated} \cong 5\ J^{net}_{normal}$	46
Cd-doped CdS vacuum sublimation	$J^{net}_{Cd\ doped\ at\ high\ T} < J^{net}_{Cd\ doped\ at\ low\ T}$ for same elapsed time	45

Cd-doped Cds, irradiated ($h\nu > E_{gap}$), vacuum sublimation	$J^{net}_{irradiated} \cong \frac{1}{5} J^{net}_{normal}$	40
	Cd precipitated	39
Pure Cds, in atomic or molecular beams of Cd and S_2	$J^{net}_{in\ S_2\ beam} \propto [S_{2(g)}]^{-1/2}$ for high $[S_2]$	48
	$J^{net}_{in\ Cd\ beam}$ relatively insensitive to impingement flux	48
Cu-doped CdS vacuum sublimation	$J^{net}_{Cu\ doped} \cong \frac{1}{2} J^{net}_{normal}$	47
Cu-doped CdS, irradiated ($h\nu > E_{gap}$), vacuum sublimation	$J^{net}_{Cu\ doped}$ insensitive to radiation	47

Cu deposited on one face, opposite face sublimated	With time J^{net} first increases to above normal rate, then decreases to approximately $\frac{1}{2} J^{net}_{normal}$	47
Pure ZnO vacuum sublimation	$J^{net}_{(0001)}$, Zn face $\cong 2.8\ J^{net}_{(000\bar{1})}$, O face	41-43

is explainable if one considers that because of atomic packing, a small intrinsic distribution of dipoles of positive orientation exists on the cadmium surface and a similar distribution of negative orientation is on the sulfur surface, both distributions being independent of the Debye-Hückel distribution.[32,33] The net effect produced by summing the dipole fields is an increase in the total field strength at the sulfur surface and a decrease in the total field strength at the cadmium surface. The observed dissimilarity in rate values are predicted by the proposed model. Leonard's data,[41] support this prediction. Less energy is supposedly needed to remove a particle from the vicinity of the weaker distribution (the cadmium surface) than from the stronger distribution (the sulfur surface).

Leonard and Searcy,[42,43] and Das, et al.[44] reported an asymmetrical free vaporization rate for zinc oxide single crystals. Leonard's data[41,43] showed that the (0001) face, the zinc face, vaporized approximately three times faster than the (000$\bar{1}$) face, the oxygen face. The zinc oxide crystal, assumed to have a Frenkel disorder, also has a negatively oriented Debye-Hückel dipole, equation (44). Since both ZnO and CdS have the same "wurtzite" crystal structure, the small surface dipoles possess identical orientation. The explanation of the asymmetry is the same as that given previously for cadmium sulfide.

Somorjai and Jepsen[45] doped single crystals of cadmium sulfide with excess cadmium in closed quartz tubes. After heating at high temperatures (900°--1100°C), the crystals were quenched to room temperature to retain their high temperature defect concentrations. The crystals

were then sublimed at temperatures near 700°C. These cadmium-doped, high conductivity crystals showed the behavior seen in Figure 9, which is also consistent with the theoretical model. Increasing the cadmium concentration by quenching from higher temperatures leads to an increase in $[V_S^{\cdot}]$. The crystals quenched from 1100°C retain a greater sulfur vacancy concentration than those quenched from 900°C. Upon sublimation at 700°C, for the same elapsed time, the crystal with the initially greater cadmium concentration has the lower rate. This conforms to the condition where the surface charge is larger, equation (41); thus, the rate is smaller. As the cadmium diffuses out to the surface the sulfur vacancy concentration decreases slowly, thereby leading to a decreased Q and the observed increase in the net rate.

For a cadmium-doped crystal of CdS, a possible reaction of the excess cadmium with the crystal is the following:

$$Cd(s) \rightleftharpoons Cd_{Cd}^{x} + V_S^{\cdot} + e' \quad . \tag{65}$$

When exposed to radiation of energy greater than the band gap energy, the formation of free metallic Cd(s) or $Cd_{Cd}^{\cdot}$ is favored.[39] The concentrations of defects are related by

$$[V_S^{\cdot}]n = Ka_{Cd} \tag{66}$$

Illumination of the crystal can therefore increase the activity of cadmium. This increase may be accompanied by a corresponding increase in $[V_S^{\cdot}]$. The occurrence of the latter possibility would lead to a decrease in the net rate, as observed under proper illumination.[47]

The illumination of sulfur-doped, low conductivity cadmium sulfide

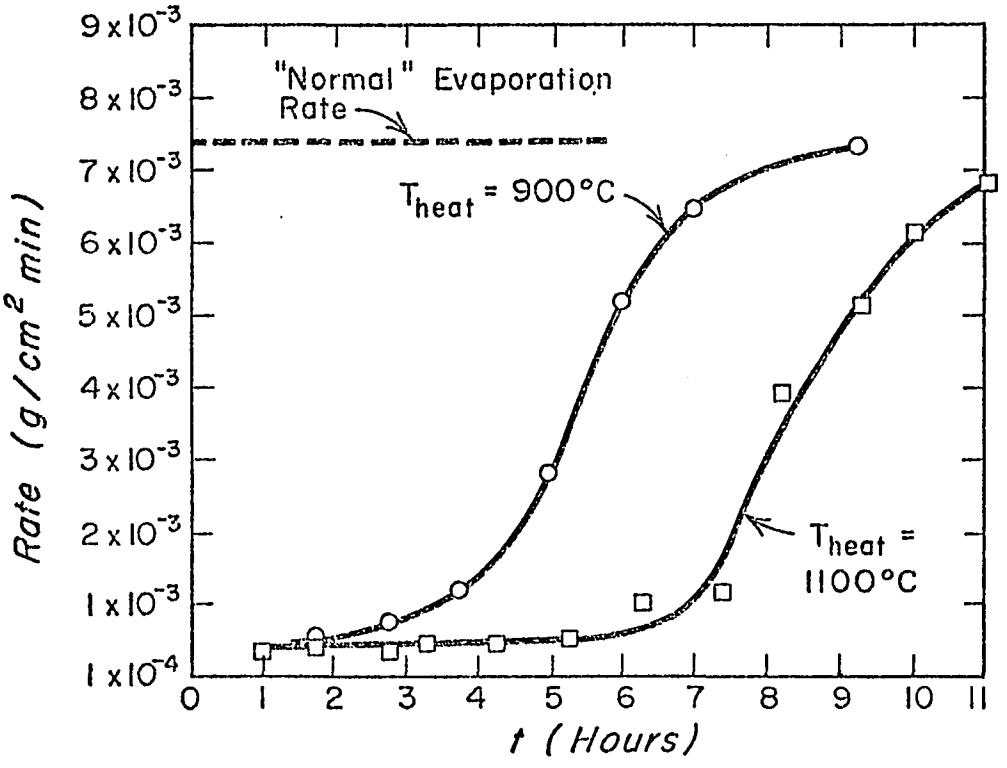

Figure 9: The evaporation rates of cadmium-doped CdS single crystal c faces as a function of time at T = 730°C.

crystals with radiation of energy greater than the band gap energy yields an increase in the hole and electron concentrations. In both cases, the increase results in much greater concentrations than the non-illuminated concentrations. The resulting increase in n and/or the decrease in $[V_S^{\cdot}]$ produces a decrease in Q, the surface charge. The total effect is an increase in the net sublimation rate. These predictions are consistent with the doped crystal observations of Somorjai and Lester.[46] The predictions for undoped crystals are also in agreement.

When crystals are doped with copper the sublimation rate should be significantly decreased. An increase in $[Cu_{Cd}']$ gives an increase in $[V_S^{\cdot}]$, predicted through equations (54) and (62), and a decrease in n, through (59) and (64). When a single crystal is doped with copper, the resulting decrease in n and increase in $[V_S^{\cdot}]$ causes an increase in Q as shown in equation (41). The observed decrease in the net sublimation rate[47] is then consistent with the proposed model.

The absence of a light effect with copper-doped crystals of cadmium sulfide is also predicted by the proposed theory. As shown by equations (58), (63), and (64) the presence of copper evidently controls both the sulfur vacancy concentration and the electron concentration. An increase in n through illumination has little effect on $[V_S^{\cdot}]$, Q, or the rate. Somorjai and Lyon,[47] reported that doping with copper makes the observed rate insensitive to light, consistent with expectation.

Somorjai and Lyon plated copper onto one surface of a single crystal and measured the net sublimation rate of the opposite face. They

observed a pulse in the sublimation rate as shown in Figure 10. The unusual pulse in the observed rate can be explained by postulating a moving dipole within the crystal. The pulse is associated with the increased sulfur vacancy concentration which approaches the vaporizing surface with the diffusing copper. With time, the $[V_S^{\cdot}]$ pulse will approach the surface bringing with it a compensating distribution which initially weakens the surface distribution potential and later strengthens it. Initially the lowered surface charge brings about an increased rate. As the dipole moves toward the surface, Q increases and the rate decreases.

Somorjai and Jepsen[40] varied the surfaced concentration of the vapor species by using molecular beams of sulfur and cadmium impinging on the sublimating surface of a cadmium sulfide single crystal. By measuring the vaporization rate as a function of the molecular beam concentration they found that the rate was proportional to the inverse square root of the sulfur flux, provided that the flux was approximately of the same order of magnitude as the net vaporization flux. Their observations shown in Figure 11 for a cadmium sulfide crystal with an impinging sulfur flux, suggest a direct suppression of the net desorption of sulfur gas. This behavior can be explained in terms of a surface concentration control rather than surface charge influenced desorption control. Sulfur atoms obtained from the impinging flux would increase the concentration of adsorbed sulfur and its activity, and this in turn could increase the concentration of sulfur adsorbed at kinks and could in turn inhibit the kinetics of desorption from

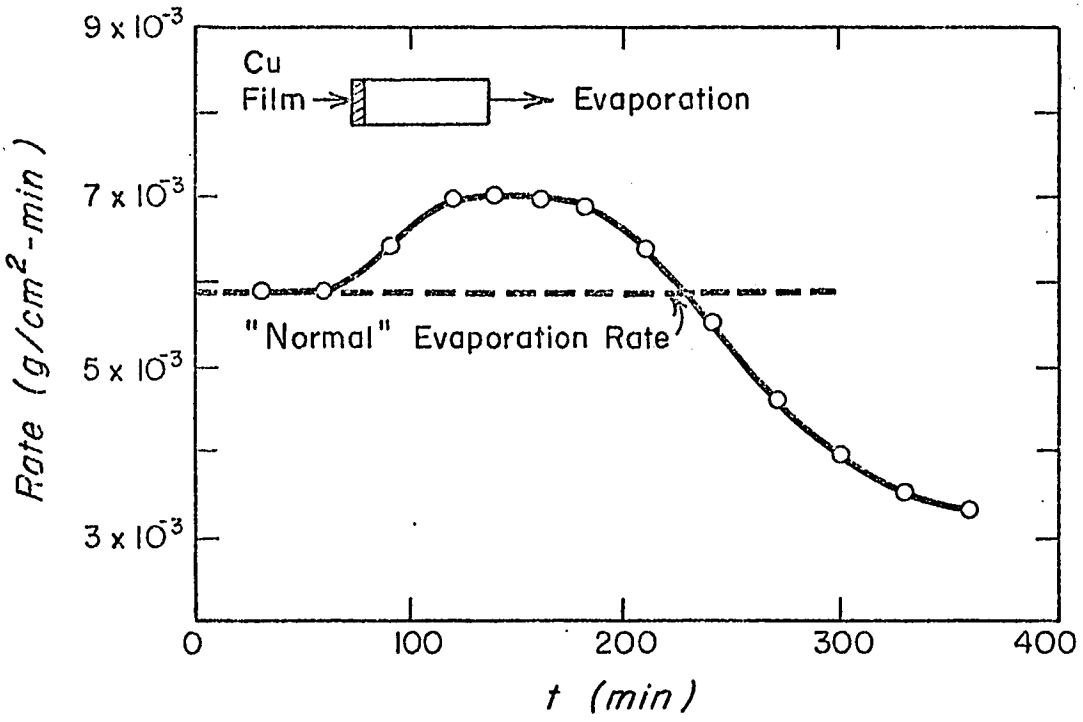

Figure 10: Evaporation rate of the (0001) face of CdS at 715°C while copper diffuses into the crystal from the $(000\bar{1})$ face.

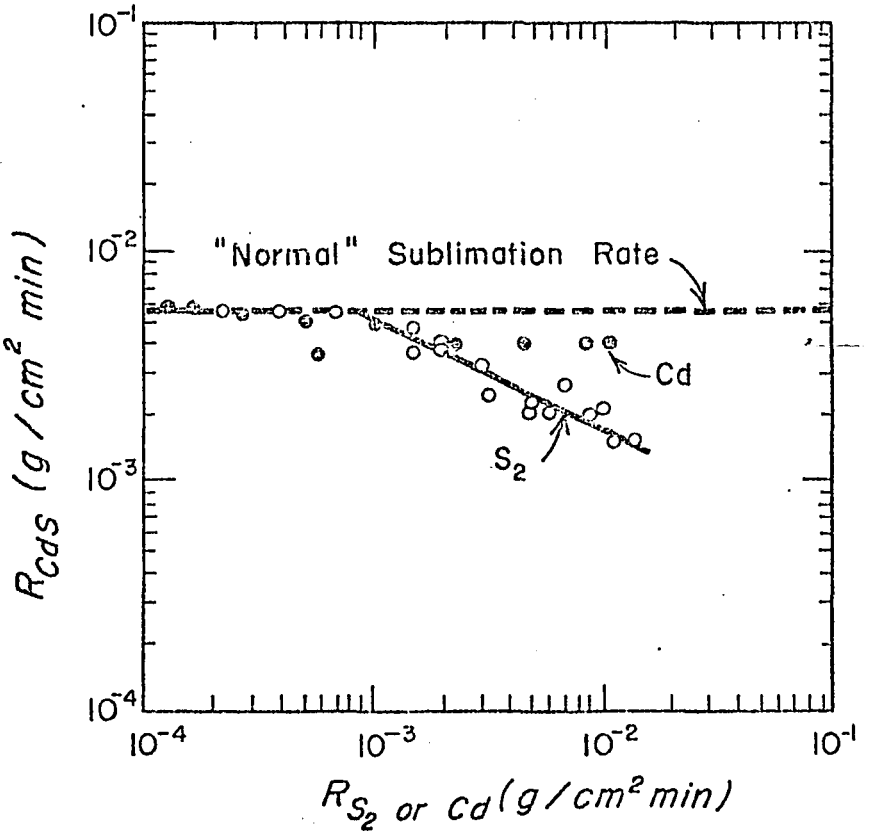

Figure 11: The evaporation rate of CdS single-crystal c face as functions of sulfur and cadmium impingement rates.

kink sites. The impinging flux can thereby override the effect of the Debye-Hückel surface charge, which, according to the proposed theory, should tend to increase rather than decrease the next vaporization rate. Somorjai and Jepsen[40] and Somorjai and Lester[46] analytically showed that the above behavior is predictable if the sulfur flux is assumed to be in equilibrium with the adsorbed species.

For short times the latter authors observed no appreciable effect on the rate when the cadmium flux was varied from below to above the net vaporization rate. However, they reported a reduced rate after long time exposures and a trend toward a reduced rate under large impingement fluxes as shown in Figure 11. In fact, they found that after long-time exposures to the cadmium and sulfur fluxes, the normal free sublimation rates could not be reestablished at once, i.e., lower values for the rates existed for some time. The increased sulfur and cadmium surface concentrations led to a diffusion of the particular species into the crystal which resulted in the observed decrease in the rate.

The metallographic studies of the evaporated surfaces revealed crystallographic features which indicate that kink formation and disconnection from kinks are influencing the sublimation mechanism.[20,21,41,43] The present analysis indicates that surface charge is influencing a step in the process, and to be consistent with the structural studies, this step is assigned as the disconnection of sublimation species from kinks. A further correlation cannot be made at this time.

EXPERIMENTAL APPARATUS AND PROCEDURE

Experimental Apparatus

The experimental apparatus for sublimation rate measurements is illustrated schematically in Figure 12, and consists of the following principal parts:

1. crystal support
2. sublimation chamber
3. furnace system
4. gas purification and control system

The crystal support is shown in Figure 13. The brass fitting supported, in cantilever manner, a fused silica tube containing the alumina specimen holder and was designed to place the holder in the constant temperature zone of the sublimation chamber. This brass fitting, with its standard-taper joint, formed a gas tight seal when inserted into a corresponding joint at the end of the fused silica furnace tube (sublimation chamber). Platinum and platinum + 10% rhodium thermocouple wires were placed through holes in the brass fitting and sealed with epoxy cement.

Several unsuccessful attempts to seal or mask off the back side of the crystal surface under investigation finally resulted in the alumina holder shown in Figure 14. This device is a 99.9% alumina tube, partially drilled out to approximately 6 mm I.D., into which a thin section of a crystal is inserted. The crystal is then held in place by a 1/4

FIGURE 12 Legend

A. Bubbler
B. Capillary flowmeter
C. Magnesium perchlorate drying agent, $Mg(ClO_4)_2$
D. Ascarite
E. BASF Katalysator, Cu / CuO with catalyst
F. Small resistance furnace for zirconia pump
G. Fused silica sublimation chamber
H. Large resistance furnace for sublimation chamber
I. Single pole relay for high-low current
J. Wheelco -Barber Coleman Series 400 on-off controller

• Stopcock

* Metering valve

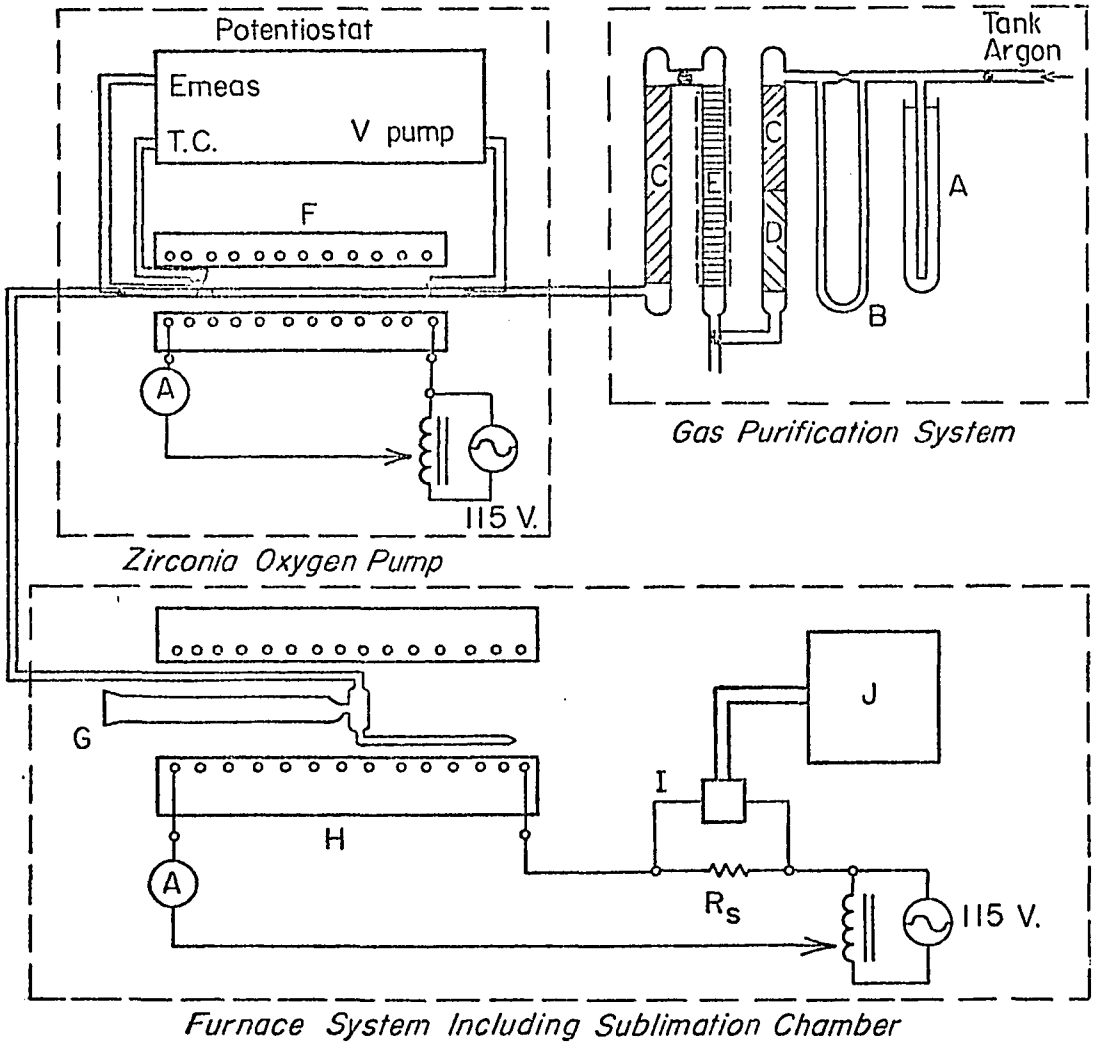

Figure 12: Schematic illustration of experimental system.

FIGURE 13 Legend

A. Pyrex standard taper joint, closed female
B. Copper cooling coils soldered to brass fitting
C. Stupakoff vacuum tight seal
D. Brass fitting with standard taper 34 / 45 joint
E. Platinum lead wire
F. Fused silica tube
G. Platinum/platinum - 10% rhodium thermo couple

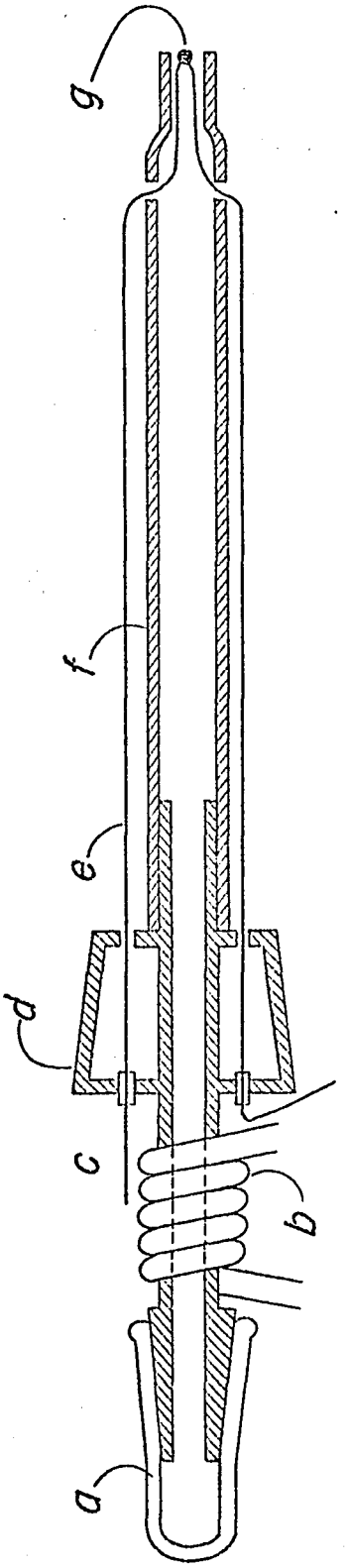

Figure 13: Crystal support.

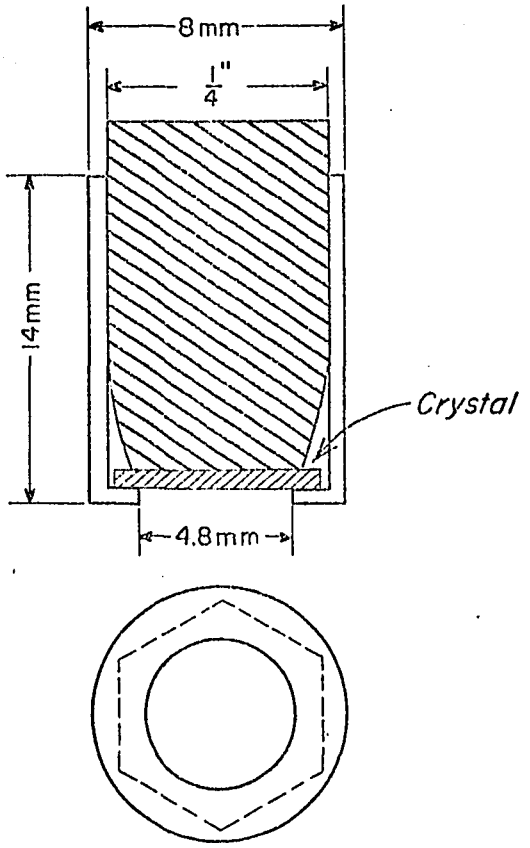

Figure 14: Alumina crystal holder.

inch diameter alumina rod which also serves to shield the back face of the crystal. After insertion into the silica tube, the Pt-Pt/10% Rh thermocouple is placed in contact with the front lip of the crystal holder.

The furnace shown in Figure 12 was a 1200°C resistance furnace purchased from Marshall Products, Inc. Temperature control was maintained by modifying a Barber-Coleman Series 400 and 340 on-off controller with a Burt[48] modulator and a high-low current supply. With the gas control system attached to the fused silica tube and Fiberfrax insulation inserted into the furnace openings, the temperature in the crystal chamber could be maintained to within 3°C of the desired temperature.

The argon purification system shown in Figure 12 was a slight modification of the system described by Rapp.[49] Prepurified argon, typicallly 99.998% pure, was purchased from Matheson Gas Products. The impurities were essentially N_2, O_2, $CO_2$and hydrocarbons such as CH_4. The incoming argon, after passing through a calibrated capillary flowmeter was purified further by passing it consecutively through anhydrous magnesium perchlorate, $Mg(ClO_4)_2$, ascarite, reduced and oxidized BTS catalyst (Cu and Cu_2O, respectively) at 250°C, and anhydrous magnesium perchlorate. Water vapor was removed by $Mg(ClO_4)_2$, while carbon dioxide and other hydrocarbons were removed by the ascarite. By previously heating the BTS Katalysator to 250°C in flowing hydrogen gas it was reduced to activated copper. This was then used to remove oxygen present in the argon. The oxidized Katalysator accomplished the removal of

hydrogen. Any remaining water vapor was removed by the final $Mg(ClO_4)_2$ tower. The resulting argon, freed of any significant H_2O, H_2, O_2, or CO_2, then passed into a special zirconia tube contained in a small tube furnace.

The oxygen pump, a 7-1/2 wt % calcia stabilized zirconia tube with its platinum electrodes is shown schematically in Figure 15. This device was used to control the oxygen activity in the argon gas passing over the crystal in the sublimation chamber. According to Yuan and Kröger[50], and experiments performed in this laboratory, a zirconia tube can be used to pump oxygen into or out of the flowing argon-oxygen gas if a voltage of appropriate sign is applied to the internal and external electrodes. The pump is described in detail below.

After passing through the zirconia pump, the argon-oxygen gas flowed into the fused silican sublimation chamber and across the exposed surface of the crystal. During sublimation, gaseous components of the crystal are carried away and condensed in the lower temperature regions of the system.

Zirconia Oxygen Pump

Solid electrolyte galvanic cells have been used in recent years to study the thermodynamic properties of many compounds. In addition, several comprehensive books and articles have been published which present summaries of ionic conduction in solids and solid electrolyte techniques.[36,51-55] Although solid electrolytic cells previously have been used successfully to monitor oxygen activities in several systems,

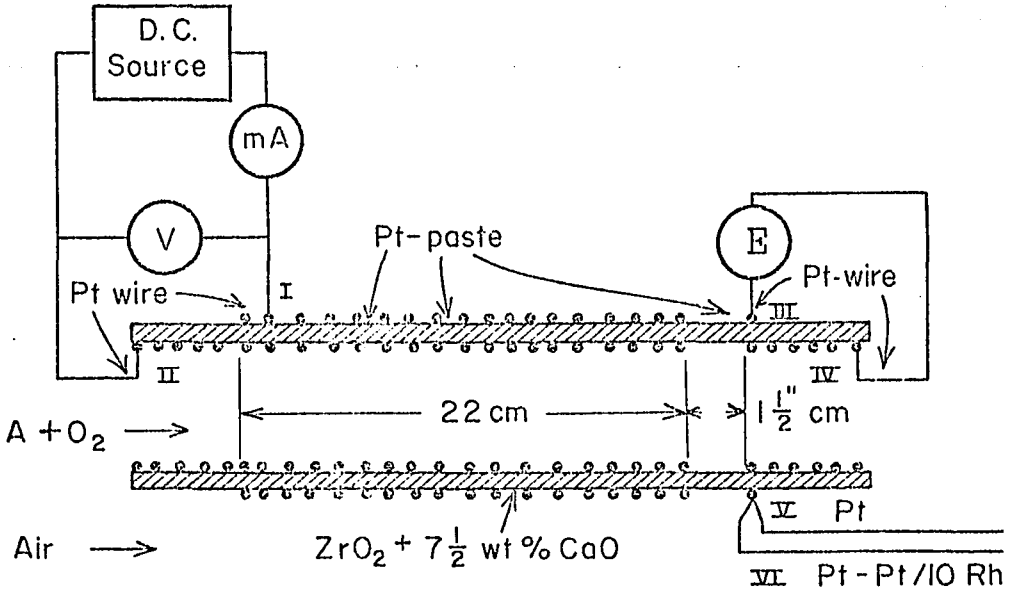

Figure 15: Zirconia oxygen pump.

Yuan and Kröger[50] first reported experiments using solid electrolytic cells based on stabilized zirconia to remove oxygen from a streaming gas. The authors investigated the effectiveness of stabilized zirconia as an oxygen pump and found that it was possible to reach oxygen pressures as low as 10^{-38} atmospheres. Since a precise determination of the oxygen partial pressure is important in our transpiration studies, further investigation of this technique has been performed in this laboratory.

The present work utilized the cell

$$P'_{O_2}, Pt \;\Big|\; \underset{\text{(Solid electrolyte)}}{ZrO_2 + CaO} \;\Big|\; \underset{\text{(Reference Electrode)}}{Pt,\ Air\ (P''_{O_2} = 0.21\ atm)}$$

where P''_{O_2} is the oxygen partial pressure in the reference gas and P'_{O_2} is the oxygen partial pressure in the flowing argon plus oxygen stream. The chemical potentials of oxygen on the two sides of the electrolyte are expressed in terms of these partial pressures by the equations

$$\mu'_{O_2} = \mu^{\circ}_{O_2} + RT\ln P'_{O_2}$$

and

$$\mu''_{O_2} = \mu^{\circ}_{O_2} + RT\ln P''_{O_2} \quad .$$

Thus, the difference in chemical potential is simply

$$\Delta G = \mu'_{O_2} - \mu''_{O_2} = RT\ln(P'_{O_2} / P''_{O_2}). \qquad (67)$$

Since the relationship between the changes in the chemical and electri-

cal potentials is given by the Nernst equation,

$$\Delta G = -nFE \tag{68}$$

where F is Faraday's constant, n is the number of electrons transported per molecule involved, and E is the electromotive force (emf), equations (67) and (68) can be combined to yield

$$E = (RT/nF)\ln (P''_{O_2} / P'_{O_2}) \quad . \tag{69}$$

In calculating this expression we have assumed that t_{ion}, the transference number of the ion, is essentially unity over the oxygen pressure range studied and that both temperature and pressure are held constant. Since two electron charges are transferred with each oxygen ion or four per molecule, equation (3) reduces to

$$E = (RT/4F)\ln (0.21 / P'_{O_2}) \tag{70}$$

for our cell. As this is written our standard state is the pure gas at unit fugacity. If a potentiometer is used to measure the open circuit voltage; the emf, the value obtained at the specified temperature yields the difference in oxygen partial pressures between the outside and inside of the zirconia tube.

If the two platinum electrodes are connected by lead wires to a constant voltage source or potentiostat, a current will result from the applied voltage according to the expression,

$$E - V_{app} = iR_{ionic} \tag{71}$$

where E is the cell emf due to difference in chemical potentials, V_{app} is the applied voltage, i is the current, and R_{ionic} is the ionic cell

resistance. When V_{app} is greater than E, a current passes from the side with the lower P_{O_2} to the side with the higher P_{O_2}. In this case, oxygen is pumped into the argon-oxygen stream. Similarly, if V_{app} is less than E, a current passes from the side of higher P_{O_2} to the side with lower P_{O_2}, and oxygen is pumped out of the flowing gas.

Figure 15 is a schematic representation of the zirconia oxygen pump. The zirconia tubes used in these experiments were high density calcia stabilized zirconia having a nominal composition given by ZrO_2 = 7-1/2 wt % CaO and were obtained from the Zirconium Corporation of America. Tubes 18 in. long x 1/4 in. O.D. x 3/16 in. I.D. were coated with electrodes made from Hanovia fluxed platinum paste, No.6082, a mixture of platinum powder and resinous material suspended in an organic solvent. Engllhard Industries, East Newark, New Jersey, sells several different types of platinum paste, and we found that the fluxed type adheres best to the zirconia. The two inner electrodes as shown in Figure 15 were made by swabbing the bore of the tube with a cotton wool plug, saturated with the platinum paste, followed by heating the tube to 850°C for approximately twenty minutes in a well ventilated furnace. Xylene was used to dilute the paste to facilitate application. Heating at this high temperature burns the carbonaceous material and leaves a thin but well bonded layer of sintered platinum on the surface of the electrolyte. Several applications were needed to produce a low resistance layer. The outer two electrodes were painted on by using a small hair brush. The outer pumping electrode was 22 cm long, while the outer measuring electrode was 1 cm long. A platinum--platinum

plus 10% rhodium thermocouple was placed immediately adjacent to the outer measuring electrode. Platinum wires were wrapped tightly around the lengths of the outer electrodes to secure good electrical contacts. The inner electrodes were also attached to platinum wires, but were clamped at the cool ends of the tube with spring steel coils. Between the pumping cell and the measuring cell, a small ceramic bead was inserted to accomplish convective mixing of the gas stream. The zirconia ceramic was attached to a standard soft glass to pyrex graded seal using Corning Glass No. 7560. This glass composition was found to have the best properties and formed a vacuum tight bond with the zirconia. The platinum wires from the inner electrodes were brought out through the soft glass to form gas tight seals.

Desired changes in the exit gas composition were obtained by applying a voltage of the appropriate polarity and magnitude across the pumping cell electrodes (I and II). The resulting change in oxygen partial pressure was monitored by a measuring cell (III and IV) downstream from the pumping cell. Simultaneous measurements of the actual pumping current, the applied voltage, the measuring cell temperature, the measuring cell emf, and the total gas flow rate were taken. Electrical measurements were made with Keithley Electrometers and a Leeds and Northrup volt potentiometer. Using these data we were able to compare the actual pumping current with the expected (theoretical) pumping current as calculated using Faraday's Law.

The relationship among the theoretical current, the gas flow rate, and the difference in oxygen partial pressures is easily determined.

Let n_{O_2} equal the number of moles of oxygen in the argon--oxygen gas mixture. Then

$$n_{O_2}\ (\text{initial}) + it/4F = n_{O_2}\ (\text{final}) \tag{72}$$

or

$$it/4F = n_{O_2}\ (\text{final}) - n_{O_2}\ (\text{initial}) \tag{73}$$

$$= \text{number of moles of } O_2 \text{ transferred through the electrolyte in time t}$$

where i is the current in amperes, t is the time in seconds, F is Faraday's constnat (96,493 coul/g-equivalent), and 4 is the number of equivalents per molecule of O_2. Dividing equation (73) by t and writing the equation in terms of partial pressures we have

$$i/4F = (n_{total}/t)\ (P_{O_2}\text{final}/P_{total}) - (n_{total}/t)\ (P_{O_2}\text{initial}/P_{total})\ . \tag{74}$$

But

$$n_{total}/t = \text{flow rate (moles/sec)} = (P_{total}V/RTt) = (P_{total}/RT)\ (V/t) \tag{75}$$

where V is the volume, R is the gas constant (0.08207 l-atm/^{o}K), and T is the absolute temperature (room temperature = 300^{o}K).

$$i/4F = (V/t)\ (1/RT)\ (P_{O_2}\ \text{final} - P_{O_2}\text{initial}); \tag{76}$$

hence,

$$i = (4F/RT)\ (V/t)\ \Delta P_{O_2} \quad . \tag{77}$$

Substituting the values for the constants and defining the flow rate as $(V/t) = G\ (cm^3/sec)$,

$$i = 15.68\ G\Delta P_{O_2}\ (\text{amperes}). \tag{78}$$

To determine the actual electrical and chemical characteristics of the oxygen pump at high temperatures, the applied voltage was used as the independent variable and i_{pump} and E_{meas} were determined experimentally. The pumping voltage was applied and both the dependent variables were monitored until steady state values were obtained. A plot of i_{pump} (calculated and observed), and E_{meas} ($-\log P_{O_2}$) versus V_{pump} are presented in Figure 16. Values for P_{O_2} initial and P_{O_2} final were determined from the open circuit emf and the steady state emf, respectively, using equation (75). Faraday's Law, equation (78), was then used to calculate the theoretical current. As observed from this plot, Faraday's Law was obeyed while oxygen was pumped in, but not while it was pumped out at high V_{pump} (low P_{O_2}). Significant polarization may possibly have taken place at high values of V_{pump}. Yanagida, Brook, and Kröger[56] found that the deviation from ohmic behaviour could be attributed to the potential drop at the cathode interface between the electrolyte and the gas. At low applied voltages, they found that the P_{O_2} dependent behaviour could be explained by the diffusion of oxygen atoms through the platinum paste electrode. At high voltages, where the behaviour was independent of P_{O_2} and polari-

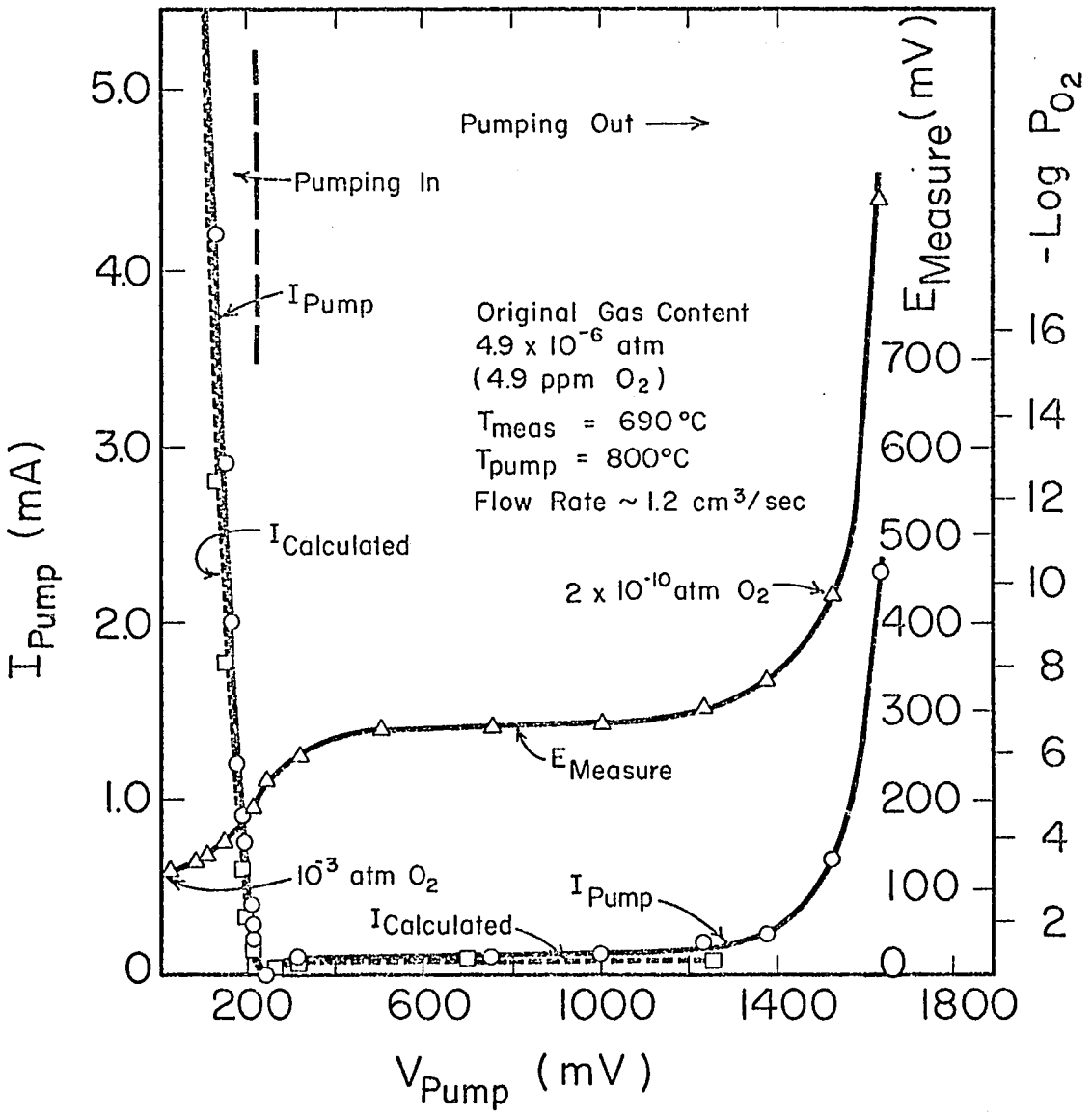

Figure 16: Characteristics of zirconia pump.

zation is strong, they concluded that the rate determining step was the combination of neutral, adsorbed oxygen atoms with neutral, vacant oxygen lattice sites to form normal, charged oxygen ions. This reaction occurs in the region adjacent to the platinum electrode, where the electrolyte becomes electronically conductive and permits the migration of electrons from the electrode.

In order to adjust and maintain a desired P_{O_2} in the exit gas, an electronic feed-back control device was developed by R. A. Rapp, Y. Agrawal, and R. Grunke. This instrument, when inserted between the measuring and pumping cell, automatically applies a variable voltage to the upstream pumping cell in response to an error signal which corresponds to the difference between the actual voltage of the down-stream open-circuit measuring cell and a desired voltage which is selected and read into the equipment. An additional refinement in the feed-back loop is the elimination of the temperature dependence of the open circuit voltage. This was done by controlling the ratio of the open circuit voltage to the absolute temperature (E_{meas}/T), since this quotient depends only on the oxygen partial pressure difference.

The control properties of the device were tested by using it to reproduce the previously mentioned, characteristic curves. However, in this later set of experiments the device was used to set a certain emf (set P_{O_2}) in the down-stream cell, and V_{pump} and i were measured. The data from the latter experiments coincide almost exactly with those shown in Figure 16. Experiments performed by Y. K. Agrawal on similar tubes also verify the effectiveness of the "potentiostat" in reproducing

the steady state curves. The agreement of the two sets of experiments makes it clear that the device works as intended and that it is possible to control the partial pressure of oxygen in a flowing gas stream by coulometric titration.

Additional measurements of P_{O_2} with another zirconia probe in the sublimation chamber farther down-stream were taken to check the accuracy of the P_{O_2} indicated by the pump measuring cell. The P_{O_2} values obtained from the probe were essentially the same as those indicated at the measuring cell. These results support the assumption that there is no electrical coupling between the pump cell and the measuring cell electrodes.

Sample Preparation

Semiconductor grade zinc oxide (ZnO) single crystals grown by and obtained from the 3M Company were used in these experiments. The crystals supplied were hexagonal needles approximately 10 mm long with a diameter of less than 6 mm. Several crystals of Lot 307, Batch 160 were bought and sections subsequently identified as S1, S2, etc. The 3M Company regularly cut the crystals with a diamond saw and lightly polished the cut surfaces with 600 grit silicon carbide abrasive paper. Leonard[41] examined similar crystals with an electron beam microprobe and reportedly found large concentrations of silicon and aluminum present. Even after etching expensively with nitric acid these amounts were present. Additional crystals were then ordered which were not polished after cutting. His analysis showed that the silicon and alum-

inum were absent. In either case, Leonard found no difference in vacuum vaporization behavior between those crystals with these large trace impurity concentrations and those without. Evidently polishing has no large effect on the vaporization rate.

Table 3 shows a typical emission spectrographic analysis of the 3M Company crystals.

The sections used in our experiments were cut from single crystals oriented so that the (0001) and (000$\bar{1}$) surfaces were exposed. The hexagonal needles were oriented with a Bond adjustable barrel holder using the method described by Wood.[57] Crystals were held on the steel stage by thermosetting plastic. The Bond holder was adjusted by trial and error until the $\langle 0001 \rangle$ direction was parallel to the x-ray beam. A Polaroid XR-7 System was used for x-ray crystallography. The procedure was very rapid and gave a precise orientation. After adjusting the crystal to within less than one degree of the $\langle 0001 \rangle$ direction, the specimen and holder were removed from the x-ray machine. The holder and sample were then placed on a precision cut-off machine and basal slices were cut using a thin diamond saw and an aqueous coolant with rust inhibitor. The cut surfaces were polished successively with 260, 400, and 600 grit silicon carbide abrasive paper until the thickness of each section was approximately 1.5 mm.

As previously mentioned in section II, the (0001) and (000$\bar{1}$) basal surfaces are not crystallographically equivalent. Mariano and Hanneman[33] investigated this difference in crystal structure along the c-axis and correlated the intensities of the zinc K adsorption edges

TABLE 3: Zinc Oxide (ZnO) Crystals as Purchased from 3M Co.
Typical Analysis

Element	Detection limit, ppm	Quantity, ppm
Ag	< 1.0	< 1.0
Cu	< 1.0	8
Cd	3	----
Ti	< 1.0	----
V	< 1.0	< 1
Ca	< 1.0	< 1
Sn	< 1.0	1.5
Mo	< 1.0	----
Be	< 1.0	----
AL	3	< 3
Bi	< 1.0	----
In	3	----
Ge	< 1.0	----
Fe	< 1.0	< 1
Cr	< 1.0	< 1
Ni	< 1.0	----
Si	5	< 5
Sb	10	----
Mg	< 1.0	< 1
Pd	3	----
Mn	< 1.0	----
B *	< 1.0	5
Te	10	----
As	10	----
Ba	3	----
Li	< 1.0	< 1
K	3	< 3
Na	< 1.0	3

* Ground in B_4C mortar and pestle

with chemical etching behavior. After using a 20 volume % nitric acid etchant, they observed hexagonal pits on the zinc surface and non-distinct hillocks on the oxygen surface. Figures 17 and 18 are optical photographs showing these surface features when the crystals are etched for 90 seconds with the nitric etchant. Figures 19 and 20 are micrographs taken with a Materials Analysis Company scanning electron microscope. From Figure 18 it is clearly evident that the chemically etched oxygen surface, $(000\bar{1})$, is really composed of crystallographic spires having at least 6 sides. We have identified those surfaces having the hexagonal pits shown in Figure 17 as zinc surfaces, (0001), in accord with the results of Mariano and Hanneman. For certain crystals these hexagonal pits were not always present under optical viewing, but the typical "pebbled" morphology (spires) of the oxygen surface always provided a means for distinguishing between the two surfaces.

Experimental Procedure

Before performing any sublimation experiments with single crystal samples, the oxygen pump control device was set to maintain the desired oxygen partial pressure, a value between 10^{-14} and 10^{-1} atmospheres. The gas flow rate was determined by adjusting the fine metering value until the pressure difference corresponded to the previously calibrated flow. The crystal support, with attached thermocouple, was placed in the furnace and tightly sealed. With an ice-water mixture as a reference, the thermocouple emf was monitored and the furnace control set point adjusted until the temperature in the sublimation chamber reached

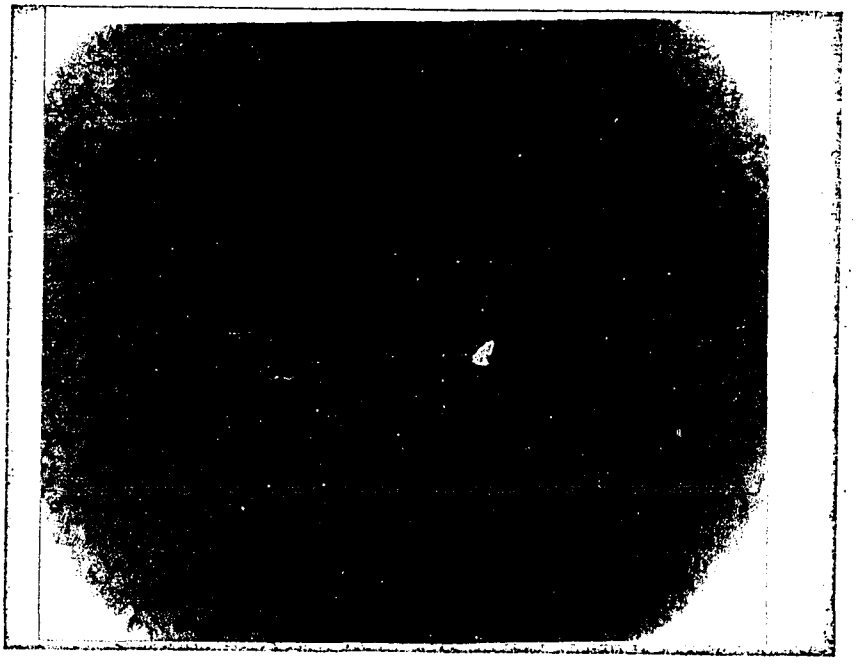

Figure 17: Zinc surface of chemically etched zinc oxide single crystal (500x, optical, 90 sec. 20 volume % nitric acid).

Figure 18: Oxygen surface of chemically etched zinc oxide single crystal (500x, optical, 90 sec. 20 volume % nitric acid).

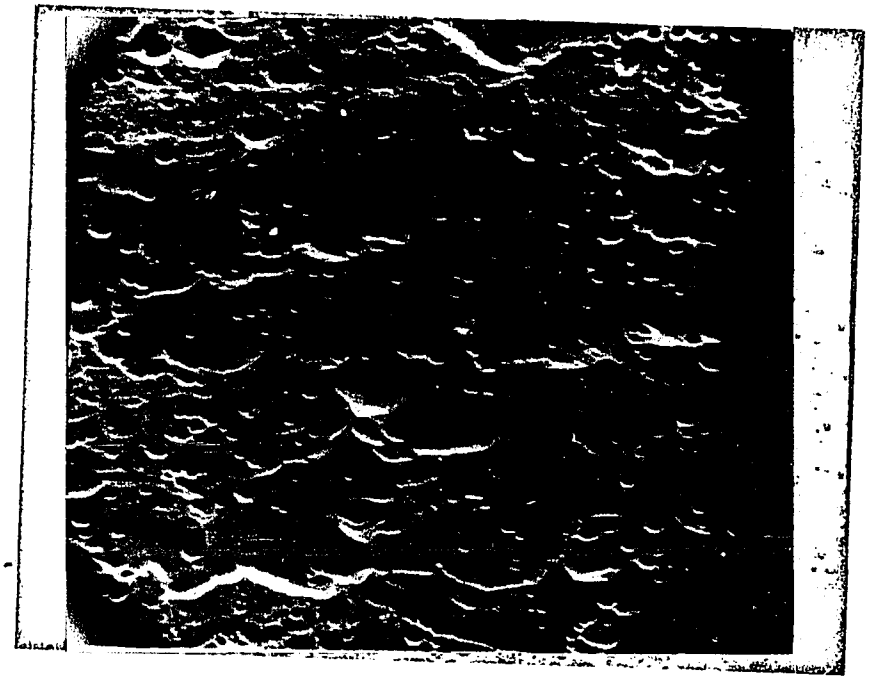

Figure 19: Zinc surface of chemically etched zinc oxide single crystal (1000x, SEM at 49° tilt, 90 sec. 20 volume % nitric acid).

Figure 20: Oxygen surface of chemically etched zinc oxide single crystal (1000x, SEM at 45° tilt, 90 sec. 20 volume % nitric acid).

a steady state value of 1100°C.

The crystal support was then removed and allowed to cool while the crystal holder was being assembled. A crystal basal slice, with the exposed surface identified as either the (0001) or the (000$\bar{1}$) face, was inserted in the holder as illustrated in Figure 14. After assembly, the crystal and holder were placed in the silica support and the thermocouple placed in contact with the lip of the holder. The completed assembly was again inserted into the furnace. The time was recorded and the temperature monitored until steady state was once more reached. Simultaneous measurements of the flowmeter pressure difference, sublimation furnace temperature, oxygen pump reference cell temperature, and oxygen pump emf were recorded.

The crystal was allowed to sublime for several days to insure an adequate mass loss. Upon removal from the furnace the entire assembly was allowed to cool for approximately five minutes, after which time, the crystal and holder were placed in a dessicator containing magnesium perchlorate. The dessicator was then taken to the electrical microbalance.

Mass Loss Determination

The actual mass lost during the sublimation experiment was determined with an Ainsworth, series 1000, electrical microbalance. The accuracy of measurements was $\pm 1 \times 10^{-5}$ gram. Since the sublimation rate can be determined by knowing the exposed area and the relative change in the mass of the crystal with time a method was devised to

measure this relative change. The mass of the crystal was compared to the mass of a standard platinum tare.

Using both pans of the balance, the standard tare was approximately equilibrated with the a set of tare weights. The mass difference, Δt, between the tare and the standard was recorded. The standard mass was replaced with the crystal and measurements again taken. The latter mass difference, Δs, was then subtracted from Δt to yield the difference, Δw, between the standard and the crystal. By using this method, we eliminated any discrepancy due to dirt or dust on the pans or change in the balance zero. Several measurements of a sample taken weeks apart support the validity of this method. Differences between the Δw's taken before and after each sublimation experiment yielded the actual mass loss which occurred.

Surface Morphology

After the mass change of the crystal was determined, it was replaced in the dessicator and transported to the scanning electron microscope. Photographs of typical surface structures were taken at 1000x magnification with a standard tilt of $\sim 45^{\circ}$. Interesting features were examined at higher and lower magnifications.

RESULTS AND DISCUSSION

Results of Sublimation Experiments

Very few kinetic studies have been reported for compounds which dissociate during sublimation. As previously mentioned, many experimental parameters can influence the sublimation behavior, and for this reason most workers attempt to reduce the variables to a minimum. Differences in crystallography (orientation) and line defect structure, equilibrium defect composition, bulk impurity concentration, surface composition, and structure, relative sublimation rates of impurity and bulk atoms, temperature, composition of the gaseous phase, and the total pressure are some of those variables which the experimentalist must consider. In order to determine the exact sequence of steps through which the solid transforms to vapor and the step which controls this transformation we must decide which of the physical and chemical parameters influences the vaporization behavior.

Figure 21 shows the transpiration sublimation rate of zinc oxide single crystal c-faces as a function of the oxygen partial pressure of the incoming gas. This data is also found in Table 4. The rate is given in grams of zinc oxide lost per square centimeter per hour. The actual measured rate is about four or five orders of magnitude lower than the average equilibrium rate calculated through the equilibrium free energy changes[58,59] and the Hertz-Knudsen-Langmuir equation. The

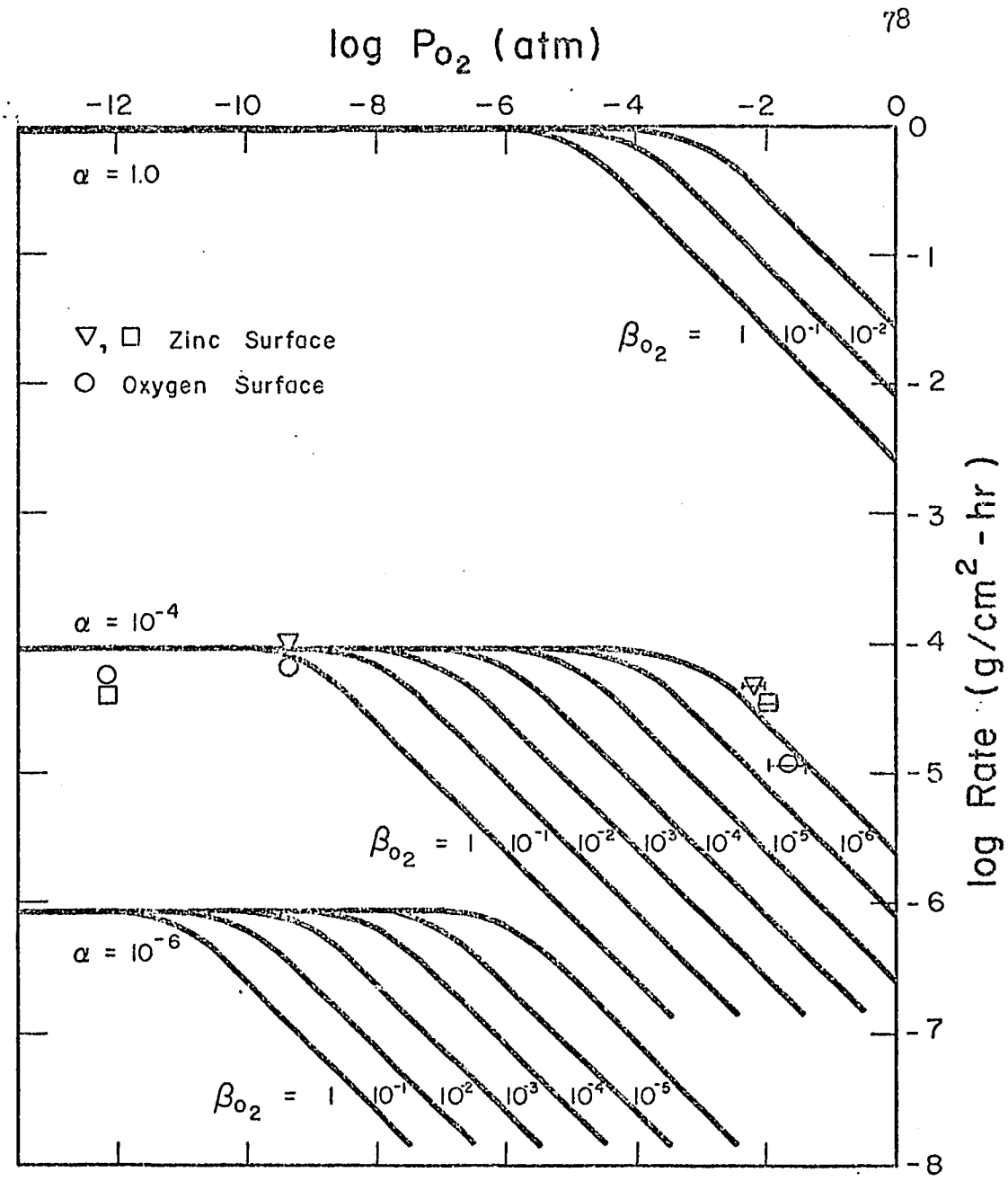

Figure 21: Sublimation rate of zinc oxide single crystal c-faces as function of oxygen partial pressure at ~1100°C.

TABLE 4: Sublimation of Zinc Oxide in Argon-Oxygen Mixture

Run	Crystal	Surface	T°C	-log Po_2^{gas} (atm)	-log Rate ($g/cm^2 hr$)
1	52	$(000\bar{1})$	1099	9.335--9.372	4.151
2	51	(0001)	1104	9.317--9.381	3.987
3	52	$(000\bar{1})$	1100	12.172	4.237
4	52	(0001)	1096	12.184	4.367
6	52	$(000\bar{1})$	1096	1.964--1.382	4.934
7	52	(0001)	1092	1.924--1.882	4.473
8	51	(0001)	1098	2.349--2.054	4.311

impinging oxygen flux may influence the rate through a change in the surface charge density or by a simple surface concentration control. Oxygen atoms obtained from the impinging gas may increase the concentration of oxygen atoms adsorbed at kinks and inhibit the kinetics of desorption from kink sites. Alternately, the impinging oxygen could interact directly with the crystal and cause a change in the defect distribution potential and thereby change the kink desorption kinetics. According to the proposed theory, this latter possibility would tend to increase the net vaporization rate.

A closer examination of the points show that in general the zinc surface (0001) vaporizes with a faster rate than the oxygen surface ($000\bar{1}$) in agreement with the vacuum sublimation results of Leonard.[41-43] The net rate for both surfaces decreases with increasing partial pressures of oxygen.

Shown in Figures 22--28 are typical surface features found for the crystal faces exposed for vaporization. Figures 21 and 22 show the zinc surfaces for oxygen partial pressures of approximately 10^{-13} atm. and 10^{-2} atm., respectively. Ledges and prominent peaks, many having definite crystallographic features, are present in both photographs. The peaks are regions on the surface which are restrained in some manner from subliming. This reasoning is based upon Figure 24 which shows the back surface of a crystal which has sublimed on the opposite face. Although the partial pressure is not known, the crystal is clearly changing in appearance. This surface evidently changes from the structure shown in Figure 20 to that shown in Figure 24. The large

Figure 22: Zinc surface of zinc oxide crystal after sublimation at ~1100°C and ~10^{-13} atm. O_2 (1000x, SEM at 45° tilt).

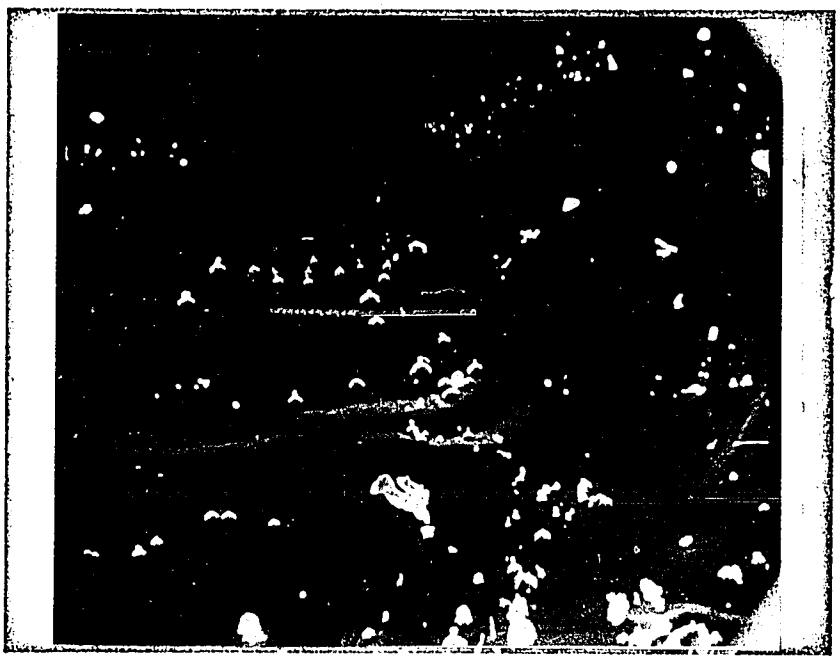

Figure 23: Zinc surface of zinc oxide crystal after sublimation at ~1100°C and ~10^{-2} atm. O_2 (1000x, SEM at 45° tilt).

Figure 24: Shielded zinc surface of zinc oxide after sublimation of oxygen surface showing peak formation (1000x, SEM at 45° tilt).

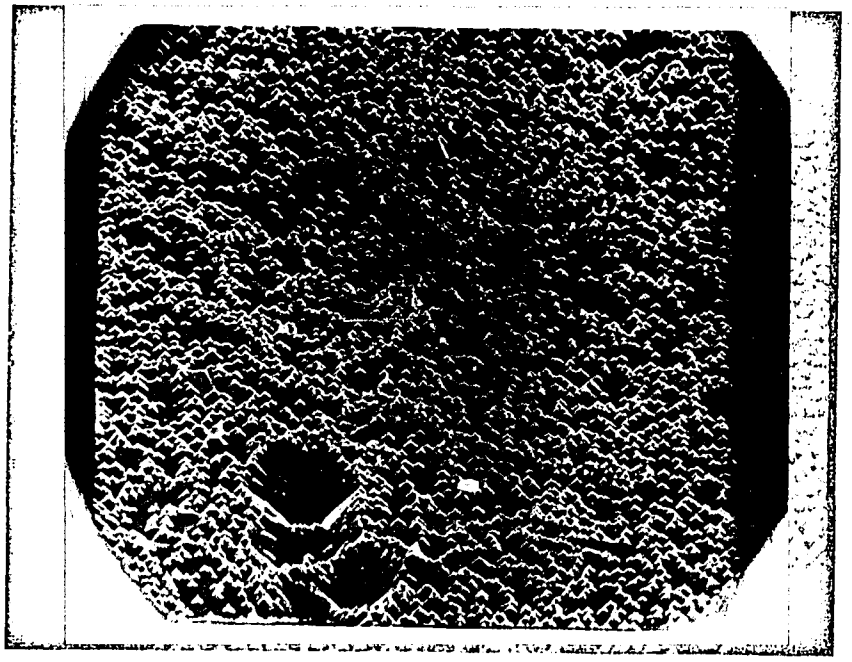

Figure 25: Zinc surface of contaminated zinc oxide crystal showing peaks formed after sublimation at ~1100°C and ~10^{-10} atm. O_2 (1000x, SEM at 45° tilt).

Figure 26: Oxygen surface of zinc oxide single crystal after sublimation at ~1100°C and ~10^{-13} atm. O_2 (1000x, SEM at 49° tilt).

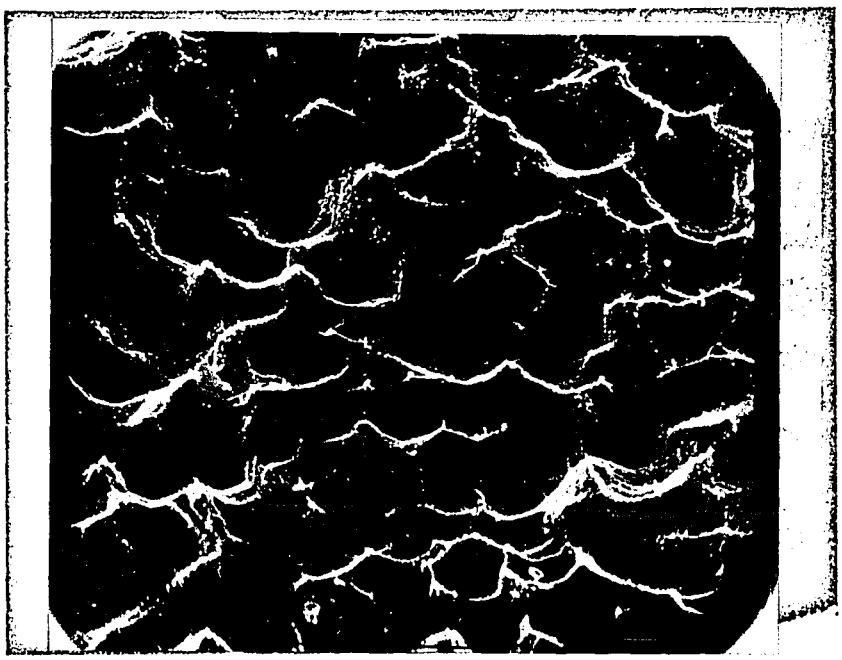

Figure 27: Oxygen surface of zinc oxide single crystal after sublimation at ~1100°C and ~10^{-10} atm. O_2 (1000x, SEM at 45° tilt).

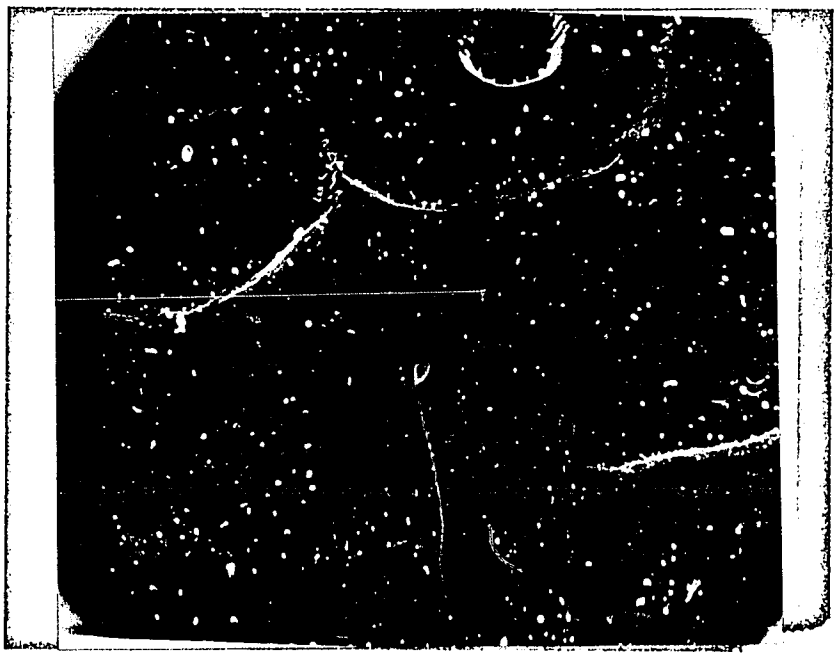

Figure 28: Oxygen surface of zinc oxide single crystal after sublimation at ~1100°C and ~10^{-2} atm. O_2 (1000x, SEM at 45° tilt).

pit on the left of the photograph is a chemical etch pit. Since these chemical pits do not contain the peaks and are sharply separated from the immediate surface before subliming, these prominent peaks are formed as the surrounding surface sublimes. The zinc surface of a contaminated crystal, having a yellow color and a lower vaporization rate under the same gas pressure as the crystal in Figure 22, is shown in Figure 25. The concentration of these spires is much larger, tending to support the contamination explanation. Figures 21 and 22 show a qualitative agreement between the observed rate and surface roughness. The number of macroscopic ledges per unit area is greater for the crystal with the higher sublimation rate and low impinging partial pressure.

Figures 26--28 show the typical oxygen surfaces of a single crystal sublimed under conditions similar to the previous experiments. There is a more striking transformation from the mountainous etched surface, as shown in Figure 21, to the hexagonally pitted surface, as shown in the last three figures. These surfaces also show a qualitative agreement between the sublimation rate and the surface structure. The number of macroscopic ledges decreases with lower oxygen partial pressure.

In contrast to the results of Leonard,[41-43] definite crystallographic features were found on both surfaces of the zinc oxide crystals examined. Whereas, he found a smooth, rolling, mountainous surface on the zinc face, we found the ledges and peaks. Oxygen surface morphologies were similar.

Discussion of Results

We shall present a phenomenological model for the vaporization of the compound MX which dissociates to form M and X_2 according to the equation

$$MX(g) \rightleftharpoons M(g) + (1/2)X_2(g) \quad . \tag{79}$$

In order to reduce the number of variables to a miminum, the analysis will be carried out for conditions of constant temperature, using a pure, single, perfect MX crystal which has a known area exposed for sublimation, and where the vapor phase contains only M or X_2. We now define the net flux of M or X_2 off the surface, J_i^{net}, as the sum of the true sublimation flux, J_i^{gross}, and the condensation flux, J_i^{cond}:

$$J_i^{net} = J_i^{gross} - J_i^{cond} \quad . \tag{80}$$

Since we can impose the congruency requirement, that the composition of the vapor coming off the crystal is the same as the composition of the crystal, we have

$$J_{MX}^{net} = J_M^{net} = 2J_{X_2}^{net} \ (\text{moles/cm}^2\text{sec}) \quad . \tag{81}$$

In general, the net flux can also be expressed using the vaporization coefficient, α_i, and the equilibrium partial pressure, P_i^*, as

$$J_i^{net} = \alpha_i P_i^*/(2\ M_i RT)^{1/2} = P_i^{expt}/(2\pi M_i RT)^{1/2} \quad . \tag{82}$$

The values of P_j^* are found by combining the congruency requirement from equation (81),

$$P_M^* = 2P_{X_2}^* (M_M/M_{X_2})^{1/2} \quad , \tag{83}$$

with the equilibrium expression from equation (82),

$$K = P_M P_{X_2}^{1/2} \quad , \tag{84}$$

and are given by

$$P_M^* = 2^{1/3} K^{2/3} (M_M/M_{X_2})^{1/6}$$

$$P_{X_2}^* = 2^{-2/3} K^{2/3} (M_{X_2}/M_M)^{1/3} \quad . \tag{85}$$

Using the expressions above, we can write

$$\begin{aligned} P_i^{expt} &= \alpha_i P_i^* - \beta_i P_i^{gas} \\ &= P_i^{surf} - \beta_i P_i^{gas} \end{aligned} \tag{86}$$

where we define β_i as the condensation coefficient of species i and P_i^{gas} as the partial pressure of the ith species in the vapor phase. Table 5 shows several conditions under which sublimation may occur.

TABLE 5: Sublimation Conditions for Thought Experiment

Condition	Explanation
(a) $P_i^* = P_i^{surf} = P_i^{gas}$	True thermodynamic equilibrium
(b) $P_i^* = P_i^{surf} = P_i^{gas}$	Adsorbed atoms in equilibrium with the crystal, no gas-solid equilibrium
(c) $P_i^* = P_i^{surf} = P_i^{gas}$	Adsorbed atoms in equilibrium with the gas, no adsorbed-solid equilibrium
(d) $P_i^* = P_i^{surf} = P_i^{gas}$	No equilibrium among species

For condition (a) we can write

$$J_M^{net} = 2J_{X_2}^{net} = J_{MX}^{net}$$

or

$$\alpha_M P_M^*/(2\pi M_M RT)^{1/2} = 2\alpha_{X_2} P_{X_2}^*/(2\pi M_{X_2} RT)^{1/2} \quad . \tag{87}$$

Since this is the congruency statement, we see that $\alpha_M = \alpha_{X_2}$. The experimental rate of mass loss can be expressed as

$$P_M^{expt}/(2\pi M_M RT)^{1/2} = P_M^{surf}/(2\pi M_M RT)^{1/2}$$

$$- \beta_{X_2} P_M^{gas}/(2\pi M_M RT)^{1/2} \tag{88}$$

thus,

$$P_M^{expt} = P_M^{surf} - \beta_M P_M^{gas} \tag{89}$$

$$P_{X_2}^{expt} = P_{X_2}^{surf} - \beta_{X_2} P_{X_2}^{gas} \quad . \tag{90}$$

Since we have imposed condition (a), these reduce to

$$P_M^{expt} = (1 - \beta_M) P_M^{gas} = \alpha_M P_M^* = P_M^* \tag{91}$$

and

$$P_{X_2}^{expt} = (1 - \beta_{X_2}) P_{X_2}^{gas} = \alpha_{X_2} P_{X_2}^* = P_{X_2}^* \quad . \tag{92}$$

Inspection of (91) and (92) shows that

$$\beta_M = \beta_{X_2} = 0 \quad . \tag{93}$$

The congruency condition (83) and the equilibrium condition (84) yield a simple relationship between the measured partial pressure of subli-

mation rate and P_i^{gas} :

$$P_M^{expt} = K(P_{X_2}^{gas})^{-1/2} \tag{94}$$

and

$$P_M^{expt} = P_M^{gas} \quad . \tag{95}$$

In terms of sublimation rate, these partial pressure dependences become

$$J_{MX}^{net} = (2\pi M_M RT)^{-1/2} K(P_{X_2}^{gas})^{-1/2} \text{ moles/cm}^2\text{sec} \tag{96}$$

and

$$J_{MX}^{net} = (2\pi M_M RT)^{-1/2} P_M^{gas} \text{ moles/cm}^2\text{sec} \tag{97}$$

In condition (b) the adsorbed species are in equilibrium with the crystal species; neither are in equilibrium with the gas species. We can again write equations (89) and (90) with P_M^{surf} and $P_{X_2}^{surf}$ replaced by P_M^* and $P_{X_2}^*$, respectively. Using the congruency relation and the equilibrium expression we have

$$(P_M^{expt} + \beta_M P^{gas}) \ (P_{X_2}^{expt} + \beta_{X_2} P_{X_2}^{gas})^{1/2} = K$$

or

$$(P_M^{expt} + \beta_M P_M^{gas}) \ (\tfrac{1}{2} P_M^{expt} (M_{X_2}/M_M)^{1/2} + \beta_{X_2} P_X^{gas})^{1/2} = K \tag{98}$$

If such an experiment is performed in vacuum with no back flux of either species, that is, if $\beta_M P^{gas} = \beta_{X_2} P_{X_2}^{gas} = 0$, then the sublimation rate will have the same partial pressure functional dependences as does

condition (a). If there is any back flux of M or X_2 species, the sublimation rate becomes a complicated function of β_M, β_{X_2}, P_M^{gas}, and $P_{X_2}^{gas}$.

Equation (98) can be solved if the proper conditions are obtained. By performing the experiment in vacuum with a known impingement flux or by subliming the crystal in a fast moving gas stream containing one of the subliming species, one can determine the condensation and evaporation coefficients. Since values for equilibrium constants are accurately known one can measure the sublimation rate as functions of P_M^{gas} and $P_{X_2}^{gas}$ and solve for the aforementioned coefficients. Equation (98) reduces to a cubic equation if only one of the gaseous species is impinging on the surface. The variables P_i^{gas} and β_i enter the coefficient of the cubic and change the magnitude and position of the theoretical curve. With proper fitting of ϕ_i and β_i one should be able to find values which coincide with the experimental points.

The third condition, where the crystal and adsorbed species are not in equilibrium but the gaseous species are in equilibrium with the latter, can be analyzed analogously. Since $P_i^{surf} = P_i^{gas}$ we can write

$$P_i^{expt} = P_i^{surf}(1 - \beta_i) \tag{99}$$

and

$$P_i^{expt} = P_i^{gas}(1 - \beta_i). \tag{100}$$

Since congruency requires $\phi_M = \phi_{X_2}$ and the equilibrium condition is

$$(P_M^{expt}/\phi_M)\,(P_{X_2}^{expt}/\phi_{X_2})^{1/2} = K\ , \tag{101}$$

we can write two equations relating P_M^{expt}, or the sublimation rate, to P_M^{gas} and $P_{X_2}^{gas}$:

$$(P^{expt}/\alpha_M)(P_{X_2}^{gas}[1 - \beta_{X_2}]/\alpha_{X_2})^{1/2} = K \qquad (102)$$

$$(P^{gas}[1 - \beta_M]/\alpha_M)(P^{expt}[M_{X_2}/M_M]^{1/2}/2\alpha_{X_2})^{1/2} = K. \qquad (103)$$

Equation (102) yields a rate which is proportional to the inverse square root of $P_{X_2}^{gas}$, $J_{MX}^{net} \sim (P_{X_2}^{gas})^{-1/2}$, while equation (103) predicts a rate proportional to the square of the inverse of P_M^{gas}, $J_{MX}^{net} \sim (P_M^{gas})^{-2}$, for all values of $P_{X_2}^{gas}$ and P_M^{gas}.

The last condition, the most complex, is the nonequilibrium among the solid, surface, and gas species. We again use congruency, but make no restrictions on the values of P_i^{expt}, P_i^{surf}, P_i^*, and P_i^{gas} other than that there is crystal equilibrium. Case (d) is very similar to case (b) and the analysis is the same. The resulting equation, like equation (98), is cubic and contains the additional factors q_i:

$$[(P_M^{expt} + \beta_M P^{gas})/\alpha_M][(P_{X_2}^{expt} + \beta_{X_2} P_{X_2}^{gas})^{1/2}/\alpha_{X_2}] = K. \qquad (104)$$

The sublimation rate in vacuum with a back flux of only X_2 is independent of $P_{X_2}^{gas}$ for very low partial pressures with respect to $P_{X_2}^*$, but changes to an inverse square root dependence for high $P_{X_2}^{gas}$. For the similar case of an impingement flux of P_M^{gas}, the rate is independent of the P_M^{gas} for very low partial pressures with respect to P_M^* and changes to a simple inverse dependence for large impingement fluxes.

In each of these cases, for condition (d), the transition from the pressure independent to pressure dependent region is smooth.

If conditions (b) and (d) are plotted as log Rate versus log P_i^{gas}, the difference between the two behaviors can easily be determined. Case (d) is simply illustrated by a downward displacement of the whole condition (b) curve with the dependent region shifted toward the lower partial pressure regions.

As we mentioned previously, Somorjai and Jepsen[40] studied the vacuum sublimation of cadmium sulfide and attempted to vary the surface concentration of the two components by using vapor beams of cadmium and sulfur. Although the authors found an inverse square root dependence of the net rate on sulfur impingement flux and could predict this functional dependence by assuming control by the sulfur surface concentration, they were unable to analyse the analogous cadmium experiment in the same manner. In their analysis of the sulfur beam experiments, essentially our condition (c), they found a discrepancy between the measured proportionality constant and that constant predicted by using a unit condensation coefficient ($\beta_{S_2} = 1$) and the Hertz-Kundsen-Langmuir equation. They postulated that a low β_{Cd} could be responsible or that the simple mechanism could be unsatisfactory. They considered other mechanisms but could find none which gave the observed power dependence with justifiable intermediate species.

Figure 29 is a reproduction of Somorjai's data for vacuum sublimation of cadmium sulfide single crystals with impinging beams of either sulfur or cadmium. Superimposed upon these experimental points are

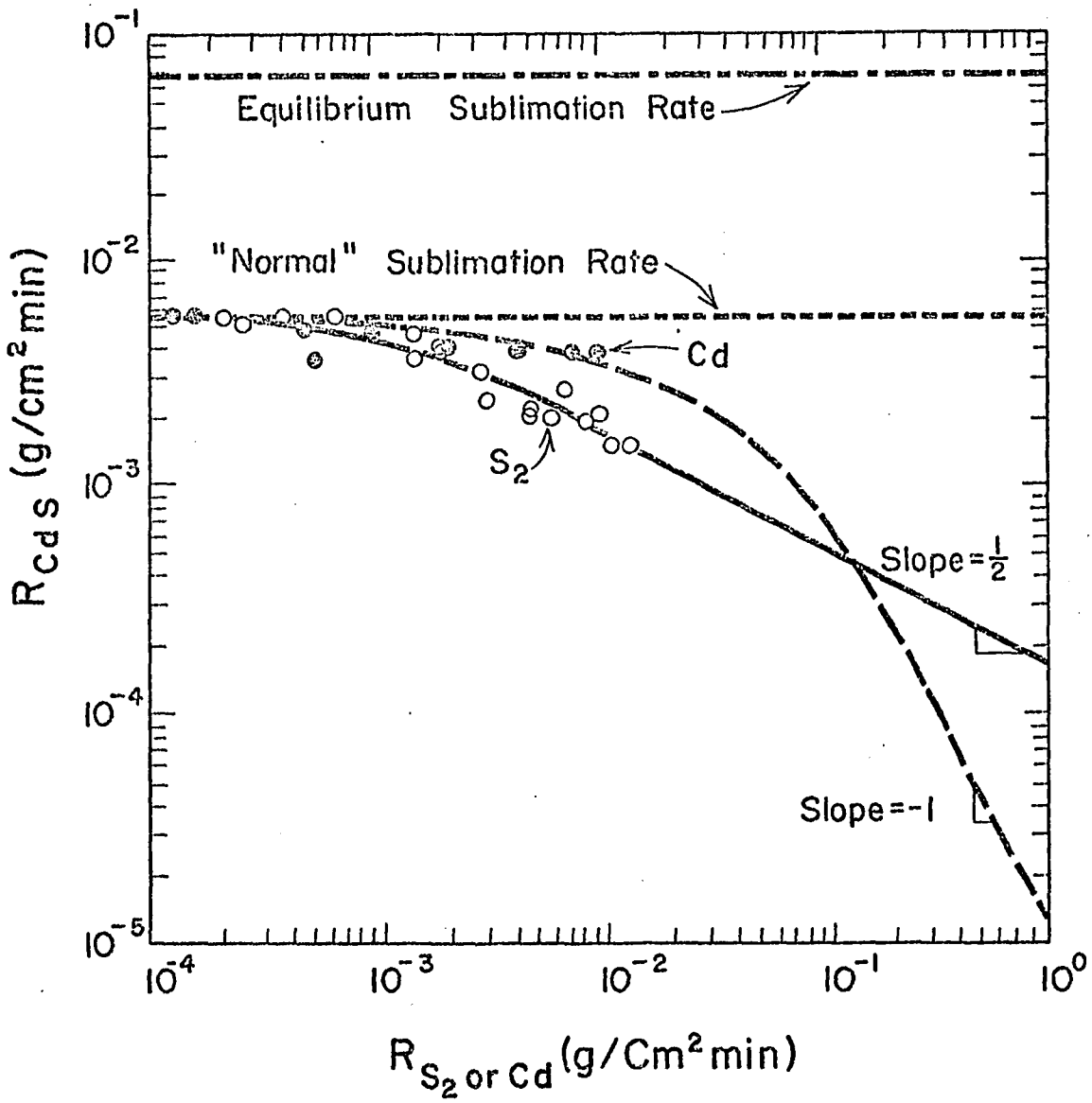

Figure 29: The evaporation rate of CdS single-crystal c face as functions of sulfur and cadmium impingement rates.

the theoretical curves which are generated by using condition (d) of our thought experiment. The fitting of the curve to the points for the S_2 impingement flux requires $\alpha_{Cd} = \alpha_{S_2} = 0.086$ and $\beta_{S_2} = 1.0$. For high S_2 fluxes the curve has a slope of -1/2, in agreement with the experimental points. For low S_2 fluxes, the rate is independent of the flux. Condition (d) has been used in the analysis since the value of α_{S_2} is much less than unity. For the data points from the cadmium experiments we have again used $\alpha_{Cd} = 0.086$ and condition (d) to generate the theoretical curve. The predicted behavior with $\beta_{Cd} = 0.30$ fits the experimental points in the low flux region, but nothing conclusive can be said for the high flux region. The very small cadmium pressure dependence of the sublimation rate does not mean that there is no agreement with theory; further high flux experiments are necessary to determine whether the slope has the negative value of unity.

These present results can mean that the rate can be controlled by the removal of only one of the species. If the sublimation is controlled by surface concentration, as is clearly the case in these experiments, the differences in β_{Cd} and β_{S_2} indicate that the rate can depend upon a mechanism involving only one species. We have predicted an increase in the rate through a decrease in the surface charge for a direct interaction of the gaseous species and the crystal. The observed functional decrease in the rate with increased surface concentration supports our suggestion that the charged distribution effect is overwhelmed.

We initially desired to determine the oxygen pressure dependence of the sublimation rate of zinc oxide in a similar manner and visually correlate the rate with changes in surface structure. Only a qualitative agreement has been found, as can be seen in Figure 21. The structural features and their subsequent changes with increasing oxygen pressure also agree qualitatively with the terrace-ledge-kink theory. A probable reason for the lack of more conclusive agreement is the diffusion complication brought about by using the transpiration technique.

The vaporization of a solid into a foreign gas can be treated in a simple manner. The transition from the solid to gas is followed by diffusion of the species into the gas. When a steady state exists the net rate can be expressed as

$$J_i^{net} = \alpha_i (P_i^{surf} - P_i^{p}) \ (2\pi M_i RT)^{-1/2} \ . \qquad (105)$$

Using Fick's first law of diffusion we can also write the rate as

$$J_i^{net} = (D_i/\delta RT) \ (P_i^{p} - P_i) \ , \qquad (106)$$

where D_i is the diffusivity of i in the foreign gas, is the thickness of the boundary layer, P_i^{p} is the vapor pressure of i at the phase boundary, and P_i is the vapor pressure at a distance δ from the surface. Equations (105) and (106) can now be combined to eliminate P_i^{p} and yield

$$J_i^{net} = \frac{\alpha_i (P_i^{surf} - P_i^{\delta}) \ (2\pi M_i RT)^{-1/2}}{1 + \dfrac{\alpha_i (RT/2\pi M_i)^{1/2}}{(D_i/\delta)}} \qquad (107)$$

Under conditions where $(D_i/\delta) \gg \alpha_i (RT/2\pi M_i)^{1/2}$, the rate is controlled by the sublimation mechanism or phase transition. When $(D_i/\delta) \ll \alpha_i (RT/2\pi M_i)^{1/2}$, diffusion of the species into the foreign gas controls the rate.

Practical limitations in controlling the oxygen partial pressure prevented us from varying the gas flow rate and the temperature to any great extent. In order to determine whether the experimental results were indicative of mechanistic or diffusion control, values for the variables in equation (107) were obtained from tables or calculated for the simple model of a gas flowing over a flat plate.[60] A very rough calculation shows that $[(D_i/\delta) = 3.3] < [\alpha_i (RT/2\pi M_{O_2})^{1/2} = 24]$; hence, the measured rate is essentially diffusion controlled.

Suggestions for Future Work

If further experiments are performed to measure the sublimation rate of zinc oxide or other ionic or near ionic oxides as a function of oxygen partial pressure, we recommend that they be done in a near vacuum. A continuously monitored mass loss, measured with an accurately calibrated helix, a torsion balance, or an electrobalance, will eliminate some of the environmental contamination encountered in these experiments. The elimination of the foreign carrier gas should reduce the gas diffusion effect. By weighing the crystal continuously, small variations in the sublimation rate will be indicated clearly. If any diffusion of the oxygen into the crystal takes place and changes the stoichiometry, there should be a definite change in the measured rate.

Small changes were not observable in the discrete measurements made in our studies. The scanning electron microscope could be utilized to a much greater extent. Using proper photogrametric techniques[61], one could measure pit sizes, slope angles, ledge heights and other surface features more distinctly. Doping and irradiation studies of the type made by Somorjai and coworkers, together with surface topography studies of the type mentioned in the theoretical development are required to test the details of the postulated charged defect distribution theory. In particular, a determination of the influence of the ledge length, L, on the sublimation rate of a vicinal surface would be significant.

SUMMARY AND CONCLUSIONS

1. Differences in the formation energies of charged defects in ionic crystals are shown to lead to the presence of a surface charge, in agreement with prior models.[24-26,28] Hence, the surface charge is explicitly related to surface kinks, and the appropriate relations between surface charge, surface structure, and bulk and vapor concentrations are developed.

2. The magnitude of the surface charge is shown to influence sublimation rates by affecting the activation energy for desorption steps and by influencing the kink concentration.

3. Predictions of the theory are compared with a series of results on II-VI compounds and are shown to be consistent.

4. Experimental transpiration results have shown that oxygen in the gas over a subliming zinc oxide crystal can decrease the rate significantly at high oxygen partial pressure values. Similar experiments by others with cadmium sulfide crystals and impingement fluxes of cadmium and sulfur have shown that the surface concentration of either specie can control the rate. Since all of the above results can be explained in terms of rate control by surface concentration, control by the charged defect distribution effect is overwhelmed under these conditions.

5. Since the sublimation rates of the zinc (0001) surfaces are larger than those for the oxygen ($000\bar{1}$) surface, we conclude that the

charged defect distribution is influencing the rate independently of the surface concentration.

6. The correlation between surface structure, impurities, and measured sublimation rates qualitatively support the terrace-ledge-kink theory of vaporization.

APPENDIX A

One layer of the charged distribution is assumed to consist of an infinite, planar, square grid of positive unit electronic charges seqarated by a distance, d, given by $d = (e/Q)^{1/2}$. A corresponding grid of negative unit electronic charges is located in the crystal at a distance λ from the surface. The energy to remove a charge in the field of this set of point charges is estimated by first calculating the total potential, ϕ, at any distance, z, normal to the planar surface. This potential is simply the sum of the potentials due to the individual charges. The potential energy of a test charge q', if placed at z, is $U(z) = q'\phi(z)$. Its potential energy at an infinite distance from the plane is $U(\infty) = q'\phi(\infty)$. Since we can define the zero of electrical potential as $\phi(\infty) = 0$, the work, U, involved in moving the test charge from z to infinity is simply

$$\Delta U = q'\phi(z) \qquad \text{(A-1)}$$

Figure 30 illustrates the assumed distribution of point charges. Figure 30(a) is a view of the square grid normal to the surface showing the neighbors and their distances from an arbitrary grid site. Figure 30 (b) is a view normal to the z-axis and represents the generalized situation.

The potential at P is

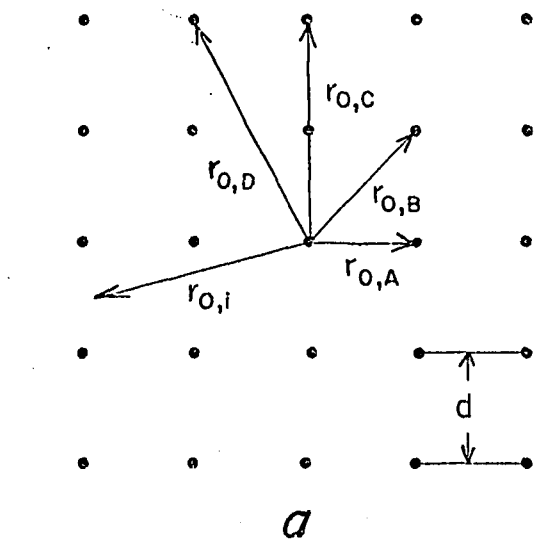

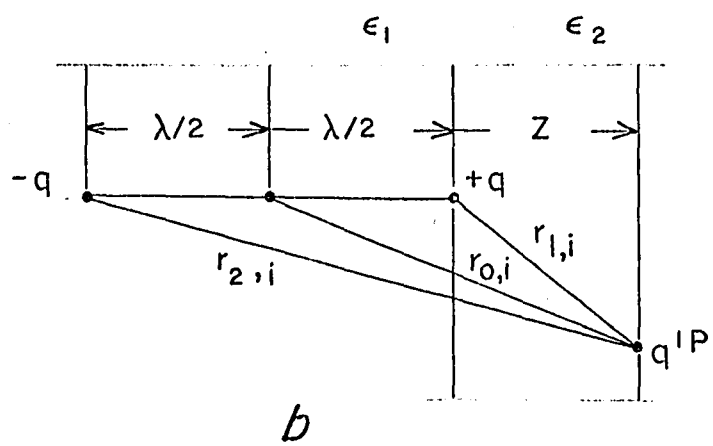

Figure 30: The distribution and geometry of point charges assumed to represent the charged defect distribution.

$$\phi(z) = (2\epsilon_1/[\epsilon_1 + \epsilon_2])(q/4\pi\epsilon_1)(1/r_{2,i} - 1/r_{1,i}) \qquad \text{(A-2)}$$

where ϵ_1 and ϵ_2 are the dielectric constants of the crystal and vacuum, respectively.[62] By inspection of Figure 30(a) we have:

$$r_{0,A} = (d^2 + [\lambda/2 + z]^2)^{1/2} = (\lambda/2 + z)(1 + d^2/[\lambda/2 + z]^2)^{1/2};$$

$$r_{0,B} = (2d^2 + [\lambda/2 + z]^2)^{1/2} = (\lambda/2 + z)(1 + 2d^2/[\lambda/2 + z]^2)^{1/2};$$

$$r_{0,C} = (4d^2 + [\lambda/2 + z]^2)^{1/2} = (\lambda/2 + z)(1 + 4d^2/[\lambda/2 + z]^2)^{1/2};$$

$$r_{0,D} = (5d^2 + [\lambda/2 + z]^2)^{1/2} = (\lambda/2 + z)(1 + 5d^2/[\lambda/2 + z]^2)^{1/2};$$

.

.

.

and $$r_{0,i} = (\lambda/2 + z)(1 + [h^2 + k^2]a)^{1/2} \qquad \text{(A-3)}$$

where

$$a = d^2/(\lambda/2 + z)^2 \quad . \qquad \text{(A-4)}$$

From the given geometry and the law of cosines,

$$r_{1,i} = (r_{0,i}^2 + [\lambda/2]^2 - 2r_{0,i}[\lambda/2]\cos\theta_{0,i})^{1/2}, \qquad \text{(A-5)}$$

$$r_{2,i} = (r_{0,i}^2 + [\lambda\sqrt{3}]^2 + 2r_{0,i}[\lambda/2]\cos\theta_{0,i})^{1/2}, \qquad \text{(A-6)}$$

and $$\cos\theta_{0,i} = (\lambda/2 + z)/r_{0,i} \quad . \qquad \text{(A-7)}$$

The general potential for one dipole can now be expressed as

$$\phi_{0,i}(z) = \left\{2q/[\epsilon_1 + \epsilon_2]4\pi\right\}\left\{1/[r_{0,i}^2 + (\lambda/2)^2 - 2(\lambda/2)(\lambda/2 + z)]\right.$$
$$\left. -1/[r_{0,i}^2 + (\lambda/2)^2 + 2(\lambda/2)(\lambda/2 + z)]\right\} \quad . \qquad \text{(A-8)}$$

The sum of all the dipole potentials for a point located a distance z above one of the grid charges is given by combining equations (A-3)--(A-8). The geometric symmetry of the array yields

$$\left\{8/[1+\delta_{hk}]\right\}\left\{2q/4\pi[\epsilon_1+\epsilon_2]\right\}\left\{[(\lambda/2+z)^2(1+[h^2+k^2]a)+(\lambda/2)^2-2(\lambda/2)(\lambda/2+z)]^{-1/2}-[(\lambda/2+z)^2(1+[h^2+k^2]a)+(\lambda/2)^2-2(\lambda/2)(\lambda/2+z)]^{-1/2}\right\} \quad \text{(A-9)}$$

for the general term in the sum where we define

$$\delta_{hk}=\begin{cases}1, \text{ if } h\neq 0,\ k=0;\ k\neq 0,\ h=0;\ \text{or } h=k;\ h,k \text{ are integers}\\ 0, \text{ if } h\neq k.\end{cases}$$

We then sum all the contributions of nearest neighbors, next-nearest neighbors, etc. to find the potential.

We assume that the dipole, atom, or ion could approach the surface no nearer than the diameter of the respective atom or ion. The actual distance of approach is uncertain since the position of the charge on a kink has not been identified. When we calculated the potential by computer, we considered all the neighboring dipoles which contributed more than 10^{-6} volts to the total potential. This cutoff occurred approximately with the three hundredth nearest neighbor.

The binding energy for the sodium chloride molecule is calculated by substituting the appropriate charges in equation (A-1) for the sodium ion and chloride ion. For example, the energy to remove the dipole is

$$\Delta U = + q\phi(2R_{Cl}\text{ion}) - q\phi(2R_{Cl}\text{ion} + r_d) \qquad \text{(A-10)}$$

where r_d is the interionic distance in the sodium chloride gas molecule.

According to Moelwyn-Hughes,[63] the dipole moment of a sodium chloride molecule can be described by

$$\mu = qr_d(1 - [\alpha_+ + \alpha_-]/r_d^3) \qquad \text{(A-11)}$$

where $(\alpha_+ + \alpha_-)$ is the molecular polarizability. We can then write the effective charge on one of the poles as

$$q_{eff} = e(1 - [\alpha_+ + \alpha_-]/r_d^3) \qquad \text{(A-12)}$$

Using values given by the author for the variables in (A-12); i.e. $r_d = 2.22\times10^{-10}$m and $(\alpha_+ + \alpha_-) = 3.27\times10^{-30}m^3$, we find

$$q_{eff} = 0.701e \qquad \text{(A-13)}$$

Thus, when we calculated the binding energy of the sodium chloride molecule, we multiplied the charge by the factor, 0.701. Other values for the polarizability,[64] $(\alpha_+ + \alpha_-) = 3.36\times10^{-30}$m, and interionic distance,[65] $r_d = 2.55\times10^{-10}$m, yield

$$q_{eff} = 0.797 \qquad \text{(A-14)}$$

We used a simplified approach suggested by West and Thompson[65] to calculate the induced dipole distance for the adsorbed sodium and chlorine atoms. They assume the charge distribution around the atom remains spherical in the presence of an applied field and the electron cloud density is uniform. In an applied field the center of negative charge shifts a distance d, from the nucleus. This distance is given by

$$d = 4\pi\epsilon_2 R_{atom}^3 (-d\phi/dz)_z/q' \qquad \text{(A-15)}$$

where q' is the charge on the nucleus. The work to remove the atom is then given by

$$\Delta U = +q'\phi(2R_{atom}) - q'\phi(2R_{atom} - d) \quad . \qquad \text{(A-16)}$$

APPENDIX B

Let N_P and N_N equal the number of geometrically positive and negative kink sites, respectively. Figures 4 and 5 indicate that each type of geometric kink can possess a cation or an anion giving N_P^+, N_P^-, N_N^+, and N_N^- different types of sites. The configurational entropy associated with the different geometric sites is calculated using Maxwell-Boltzmann statistics.

A straight ledge viewed from the right can have N_P and N_N geometric kink sites. When this ledge is viewed from the left, the N_P sites become N_N sites and conversely. In either case the number of positive sites equals the number of negative sites,

$$N_P = N_N \tag{B-1}$$

or

$$N_P^+ + N_P^- = N_N^+ + N_N^-$$

By a similar symmetry argument we have

$$N_P^+ = N_N^+ \tag{B-2}$$

and

$$N_P^- = N_N^- \tag{B-3}$$

where N_P^+ is the mirror image of N_N^+, and N_N^- is the image of N_P^-. Equation (45) can be rewritten as

$$(N_P^+ + N_N^+) - (N_N^- - N_P^-) = \frac{Q}{eL} \tag{B-4}$$

From the combination of equations (45) and (B-1) to (B-4) expressions for N_N^+ and N_P^+ can be found,

$$N_N^+ = \frac{Q}{2eL} + N_P^- \tag{B-5}$$

$$N_P^+ = \frac{Q}{2eL} + N_N^- \tag{B-6}$$

We now distribute the four types of sites on the N available sites using Maxwell-Boltzmann statistics. The N_P^+ sites can be distributed on the N available sites in

$$\Omega_{P^+} = \frac{N!}{(N-N_P^+)!\ N_P^+!} \tag{B-7}$$

possible ways. Likewise, the N_P^-, N_N^+, and N_N^- sites can be distributed in

$$\Omega_{P^-} = \frac{N!}{(N-N_P^-)!\ N_P^-!} \tag{B-8}$$

$$\Omega_{N^+} = \frac{N!}{(N-N_N^+)!\ N_N^+!} \tag{B-9}$$

and

$$\Omega_{N^-} = \frac{N!}{(N-N_N^-)!\ N_N^-!} \tag{B-10}$$

possible ways, respectively. Using the assumption that the number of available sites, N, is much greater than any particular type of site, and by applying Stirling's approximation, [$\ln x! \cong x\ (\ln x - 1)$], one finds

$$\ln\Omega_P^+ \cong -N_P^+\ (\ln N_P^+ - 1) \quad . \tag{B-11}$$

The configurational entropy is given by

$$S_{conf.} = -k \left\{ N_P^+ (\ln N_P^+ - 1) + N_P^- (\ln N_P^- - 1) + N_N^+ (\ln N_N^+ - 1) + N_N^- (\ln N_N^- - 1) \right\}. \quad \text{(B-12)}$$

For N_{pr} pairs of kinks we have

$$N_{pr} = N_P^+ + N_P^- = N_N^+ + N_N^- \quad \text{(B-13)}$$

The differentials of equations (B-5), (B-6) and (B-13) enable us to minimize the total free energy. Writing the free energy of the ledge as

$$F = F_I + 2U_k N_{pr} - TS_{conf.} \quad \text{(B-14)}$$

where $2U_k$ is the energy to form a kink pair and F_I contains all other contributions independent of the number of kink pairs, we can minimize F with respect to the number of kink pairs and find the concentrations of the particular types of sites:

$$\delta F = 2U_k \delta N_{pr} + kT \left(\delta N_P^+ \ln N_P^+ + \delta N_P^- \ln N_P^- + \delta N_N^+ \ln N_N^+ + \delta N_N^- \ln N_N^- \right) . \quad \text{(B-15)}$$

At equilibrium

$$\frac{\delta F}{\delta N_{pr}} = 0; \quad \text{(B-16)}$$

hence, by substituting the differentials into equation (B-15) with condition (B-16) applied, we obtain

$$N_P^+ N_N^- = \exp\left(\frac{-2U_k}{kT}\right) \quad . \tag{B-17}$$

By symmetry,

$$N_N^+ N_P^- = \exp\left(\frac{-2U_k}{kT}\right) \quad . \tag{B-18}$$

Equations (B-5) and (B-6) allow us to express the concentration of each type of kink in terms of the charge on the surface:

$$N_P^+ \left(N_P^+ - \frac{Q}{2eL}\right) = \exp\left(\frac{-2U_k}{kT}\right) \quad , \tag{B-19}$$

$$N_P^- \left(N_P^- + \frac{Q}{2eL}\right) = \exp\left(\frac{-2U_k}{kT}\right) \quad , \tag{B-20}$$

$$N_N^+ \left(N_N^+ - \frac{Q}{2eL}\right) = \exp\left(\frac{-2U_k}{kT}\right) \quad , \tag{B-21}$$

and

$$N_N^- \left(N_N^- + \frac{Q}{2eL}\right) = \exp\left(\frac{-2U_k}{kT}\right) \quad . \tag{B-22}$$

By invoking the symmetry argument again

$$N_P^+ = N_N^+ = 1/2\ X^+ \tag{B-23}$$

and

$$N_P^- = N_N^- = 1/2\ X^- \quad . \tag{B-24}$$

Then the concentrations of positively and negatively charged kinks can be related to the surface charge by combining equations (B-19), (B-20), (B-23), and (B-24) to give:

$$X^+ X^- = 4 \exp\left(\frac{-2U_k}{kT}\right) \tag{B-25}$$

or or

$$X^{+}\left(X^{+} - \frac{Q}{e\,L}\right) = 4 \exp\left(\frac{-2U_k}{kT}\right) \qquad \text{(B-26)}$$

and

$$X^{-}\left(X^{-} + \frac{Q}{e\,L}\right) = 4 \exp\left(\frac{-2U_k}{kT}\right) \qquad \text{(B-27)}$$

where U_k is the kink formation energy.

REFERENCES

1. Hertz, H., Ann. Phys. (Leipzig) 17, 177 (1882).

2. Knudsen, M., Ann. Phys. (Leipzig) 47, 697 (1915).

3. Langmuir, I., Phys. Rev. 2, 329 (1913).

4. Volmer, M., and I. Estermann, Z. Physik 7, 1 (1921).

5. Hartek, P., Z. Physik. Chem. 134, 1 (1928).

6. Eucken, A., Metallwirtshaft 15, 2763 (1936).

7. Hirth, J. P., and G. M. Pound, J. Chem. Phys. 26, 1216 (1957).

8. Hirth, J. P., and G. M. Pound, Progr. Materials Sci. 11, 92 (1963).

9. Frank, F. C., in Growth and Perfection of Crystals, edited by R. H. Doremus, B. W. Roberts, and D. Turnbull (John Wiley and Sons, New York, 1958), p.3.

10. Cabrera, N., Disc. Faraday Soc. 28, 16 (1959).

11. Kossel, W., Nach Ges. Wiss. Gottingen, 135 (1927).

12. Stranski, I. N., Z. Physik. Chem. 136, 259 (1928).

13. Stranski, I. N., Z. Physik. Chem. 11, 421 (1931).

14. Volmer, M., Kinetik der Phasenbildung (Steinkopff, Dresden and Leipzig, 1939).

15. Volmer, M., and I. Estermann, Z. Physik 7, 13 (1921).

16. Kossel, W., Naturwiss. 18, 901 (1930).

17. Burton, W. K., N. Cabrera, and F. C. Frank, Phil. Trans. Roy. Soc. (London) 243A, 299 (1951).

18. Knacke, O., and I. N. Stranski, in Progr. Metal Phys. 6, 181 (1956).

19. Glasstone, S., K. J. Laidler, and H. Eyring, Theory of Rate Processes (McGraw-Hill Book Co., New York, 1941).

20. Munir, Z. A., and J. P. Hirth, J. Appl. Phys. 41, 2697 (1970).

21. Munir, Z. A., L. S. Seacrist, and J. P. Hirth, Surface Sci. 28, 357 (1971).

22. Knacke, O., I. N. Stranski, and G. Wolff, Z. Elektochem. 56, 476 (1952).

23. Hirth, J. P., and J. Lothe, Theory of Dislocations (McGraw-Hill Book Co., New York, 1968).

24. Lehovec, K., J. Chem. Phys. 21, 1123 (1952).

25. Kliewer, K. L., and J. S. Köehler, Phys. Rev. 140, A1226 (1965).

26. Poeppel, R. B., and J. M. Blakely, Surface Sci. 15, 507 (1969).

27. Kröger, F. A., and H. J. Vink, Solid State Phys. 3, 310 (1956).

28. Lifshitz, I. M., A. M. Kossevich, and Ya. E. Geguzin, J. Phys. Chem. Solids 28, 783 (1967).

29. Rushbrooke, G.S., Introduction to Statistical Mechanics (Clarendon Press, Oxford, England, 1949).

30. Kusch, P., in Condensation and Evaporation of Solids, edited by E. Rutner et al. (Gordon and Breach, New York, 1964), p.87.

31. Eisenstadt, M., G. M. Rothberg, and P. Kusch, J. Chem. Phys. 29, 797 (1958).

32. Lester, J. E., Ph.D. Dissertation, University of California, Berkeley (1967).

33. Mariano, A. N., and R. E. Hanneman, J. Appl. Phys. 4, 384 (1963).

34. Gatos, H. C., J. Appl. Phys. 32, 1232 (1961).

35. Boswaram, I. M., in Mass Transport in Oxides, edited by J. B. Wachtman, Jr. and A. D. Franklin (N. B. S. Special Publications 296 August, 1968).

36. Kröger, F. A., The Chemistry of Imperfect Crystals, (North-Holland Publishing Co., Amsterdam, 1964).

37. Kröger. R. A., H. J. Vink, and J. van den Boomgaard, Z. Phys. Chem. 203, 1 (1954).

38. Bube, R. H., Photoconductivity of Solids (John Wiley & Sons, Inc., New York, 1960).

29. Somorjai, G.A., Surface Sci. 2, 298 (1964).

40. Somorjai, G.A., and D. W. Jepsen, J. Chem. Phys. 41, 1389 (1964).

41. Leonard, R. B., Ph.D. Dissertation, University of California, Berkeley (1970).

42. Leonard, R. B., and A. W. Searcy, J. Chem. Phys. 50, 5419 (1969).

43. Leonard, R. B. and A. W. Searcy, J. Appl. Phys. 42, 4047 (1971).

44. Das, B. N., C. B. Lamport, A. A. Menna, and G. A. Wolff, Fed. Sci. Tech. Infor. AD682518, AFML-WPAFB (1968).

45. Somorjai, G. A. and D. W. Jepsen, J. Chem. Phys. 41, 1394 (1964).

46. Somorjai, G. A. and J. E. Lester, J. Chem. Phys. 43, 1450 (1965).

47. Somorjai, G. A. and H. B. Lyon, J. Chem. Phys. 43, 1456 (1965).

48. Burt, J. G., J. Electrochem, Soc. 117, 267 (1970).

49. Rapp, R. A., Trans. Met. Soc. A.I.M.E. 227, 371 (1963).

50. Yuan, D., and F. A. Kröger, J. Electrochem. Soc. 116, 594 (1969).

51. Mott, N. F., and R. W. Gurney, Electronic Processes in Ionic Crystals, 2nd cd (Oxford, 1948).

52. Lidiard, A. B., Handbuch der Physik XX (Springer Publ., Berlin, 1957), p.246.

53. Wagner, C., Proc. Intern. Comm. Electrochem. Therm. Kinetics (CITCE), 7th meeting Lindan (1955) (Butterworth Scientific Publ., London, 1957).

54. Alcock, C. B., Electromotive Force Measurements in High Temperature Systems (Inst. of Mining and Metallurgy Publications, London, 1968).

55. Rapp, R. A., and D. A. Shores, in Techniques of Metals Research, Vol. IV, Part 2, edited by R. A. Rapp (John Wiley & Sons, Inc., New York, 1970), p.123.

56. Yavagida, H., R. J. Brook, and F. A. Kröger, J. Electrochem. Soc. 117, 593 (1970).

57. Wood, E. A., Crystal Orientation Manual (Columbia University Press, New York, 1963).

58. Wilder, T. C., Trans. Met. Soc., A.I.M.E. 245, 1370 (1969).

59. Darken, L. S., and R. W. Gurry, Physical Chemistry of Metals (McGraw Hill Book Co., New York, 1963), p.228.

60. Bird, R. B., W. E. Stewart, E. N. Lightfoot, Transport Phenomena (John Wiley, New York, 1966), p.25.

61. Ghosh, S. K., Photogrametric Engineering 2, 187 (1971).

62. Weber, E., Electromagnetic Theory (Dover Publications, Inc., New York, 1965) p.218.

63. Moelwyn-Hughes, E. A., Physical Chemistry (Cambridge University Press, London, 1947), p. 592.

64. Tessman, J. R., A. H. Kahn, and W. Shockley, Phys. Rev. 92, 890 (1953).

65. Greenwood, N. N., Ionic Crystals, Lattice Defects and Nonstoihiometry, (Butterworth & Co. Ltd. Norwich, 1968), p.16.

66. Wert, C. A. and R. M. Thomson, Physics of Solids (McGraw Hill Book Co., New York, 1964), p.308.